Electronic Supplementary Information (ESI) for

Cascade approach to hetero-pentanuclear manganese-oxide clusters in polyoxometalates and their single-molecule magnet properties†

Kosuke Suzuki, Rinta Sato, Takuo Minato, Masahiro Shinoe, Kazuya Yamaguchi and Noritaka Mizuno*

Department of Applied Chemistry, School of Engineering, The University of Tokyo

7-3-1 Hongo, Bunkyo-ku, Tokyo, 113-8656, Japan.

Email: tmizuno@mail.ecc.u-tokyo.ac.jp

Experimental details

Bond valence sum (BVS) calculations: The BVS values were calculated by the expression for the variation of the length r_{ij} of a bond between two atoms i and j in observed crystal with valence V_i:

$$V_i = \sum_j \exp\left(\frac{r_0' - r_{ij}}{B}\right)$$

where B is constant equal to 0.37 Å, r'_0 is bond valence parameter for a given atom pair.[S1]

Analysis of Magnetic data: The magnetic interactions were analyzed by fitting the temperature-dependence of magnetic susceptibilities with the following isotropic spin Heisenberg–Dirac–Van Vleck Hamiltonian (Eq S1) where J_1 and J_2 represent exchange interactions of M–Mn and Mn–Mn, respectively (Figures 2, S12):

$$H = -2J_1(S_{\mathrm{M}} \cdot S_{\mathrm{Mn1}} + S_{\mathrm{M}} \cdot S_{\mathrm{Mn2}} + S_{\mathrm{M}} \cdot S_{\mathrm{Mn3}} + S_{\mathrm{M}} \cdot S_{\mathrm{Mn4}}) - 2J_2(S_{\mathrm{Mn1}} \cdot S_{\mathrm{Mn2}} + S_{\mathrm{Mn3}} \cdot S_{\mathrm{Mn4}}) \quad \text{(Eq S1)}$$

The g values for Fe(III), Ni(II), Mn(III), Cu(II) were fixed to 2, and the g value for Co(II) was optimized.

Synthesis of Mn5: To an acetone solution (10 mL) of $Mn(acac)_3$ (27.1 mg, 77.3 μmol, 5 equiv. with respect to $TBA_4H_6[A\text{-}\alpha\text{-}SiW_9O_{34}]\cdot 2H_2O$), $TBA_4H_6[A\text{-}\alpha\text{-}SiW_9O_{34}]\cdot 2H_2O$ (100 mg, 30.9 μmol) was added, and the resulting solution was stirred for 2 h at room temperature (ca. 20°C). Then, diethyl ether (30 mL) was added. Dark brown precipitates formed were filtered off, followed by recrystallization from a mixed solvent of 1,2-dichloroethane and ethyl acetate. The brown crystals of **Mn5** suitable for X-ray crystallographic analysis were obtained (58 mg, 58% yield based on $TBA_4H_6[A\text{-}\alpha\text{-}SiW_9O_{34}]\cdot 2H_2O$). **Mn5** can also be synthesized by the following method: To a 1,2-dichloroethane solution (10 mL) of $\mathbf{I_{Mn}}$ ($TBA_7H_{10}[Mn(A\text{-}\alpha\text{-}SiW_9O_{34})_2]\cdot 3H_2O$; 243 mg, 39 μmol), $Mn(acac)_3$ (54 mg, 156 μmol, 4 equiv. with respect to $\mathbf{I_{Mn}}$) was added, and the resulting solution was stirred for 5 h at room temperature (ca. 20°C). Then, diethyl ether (20 mL) was added. Dark brown

precipitates formed were filtered off, followed by recrystallization from a mixed solvent of 1,2-dichloroethane and diethyl ether. The brown crystals of **Mn5** suitable for X-ray crystallographic analysis were obtained (183 mg, 72% yield based on $\mathbf{I_{Mn}}$). Elemental analysis, calcd (%) for $C_{114}H_{262}Cl_2Mn_5N_7O_{72}Si_2W_{18}$ ($TBA_7H_2[Mn_5O_2(A\text{-}\alpha\text{-}SiW_9O_{34})_2]\cdot 2H_2O\cdot C_2H_4Cl_2$): C, 20.76; H, 4.00; N, 1.49; Si, 0.85; Mn, 4.17; W, 50.18. Found: C, 20.30; H, 3.93; N, 1.20; Si, 0.89; Mn, 4.48; W, 50.00. Positive-ion MS (CSI, acetone): *m/z* 3472 (calcd. 3472) $[TBA_9H_2Mn_5O_2(SiW_9O_{34})_2]^{2+}$, 6702 (calcd. 6702) $[TBA_8H_2Mn_5O_2(SiW_9O_{34})_2]^{+}$. IR (KBr pellet, cm^{-1}): 1700, 1380, 1153, 1107, 1014, 990, 957, 934, 923, 709, 669, 614, 534, 480, 410, 376, 344, 333, 262, 255, 269.

Synthesis of $\mathbf{I_{Ni}}$: To $Ni(acac)_2\cdot 2H_2O$ (9.0 mg, 30.9 μmol) in a mixed solvent of acetone and water (5.76/0.24 mL), $TBA_4H_6[A\text{-}\alpha\text{-}SiW_9O_{34}]\cdot 2H_2O$ (200 mg, 61.8 μmol, 2.0 equiv. with respect to $Ni(acac)_2$) was added, and the resulting solution was stirred for 5 h at room temperature (ca. 20°C). Then, diethyl ether (20 mL) was added. Pale green precipitates formed were filtered off (164 mg), followed by recrystallization from a mixed solvent of 1,2-dichloroethane and diethyl ether. The pale green crystals of $\mathbf{I_{Ni}}$ suitable for X-ray crystallographic analysis were obtained (146 mg, 72% yield based on Ni). Elemental analysis, calcd (%) for $C_{114}H_{271}Cl_2N_7NiO_{70}Si_2W_{18}$ ($TBA_7H_{11}[Ni(A\text{-}\alpha\text{-}SiW_9O_{34})_2]\cdot 2H_2O\cdot C_2H_4Cl_2$): C, 21.54; H, 4.30; N, 1.54; Si, 0.88; Ni, 0.92; W, 52.07. Found: C, 21.40; H, 4.25; N, 1.54; Si, 0.87; Ni, 0.90; W, 52.27. Positive-ion MS (CSI, 1,2-dichloroethane): *m/z* 3308 (calcd. 3308) $[TBA_9HNi(SiW_9O_{31})(SiW_9O_{32})]^{2+}$, 6427 (calcd. 6427) $[TBA_8H_7Ni(SiW_9O_{33})_2]^{+}$. IR (KBr pellet, cm^{-1}): 2962, 2935, 2874, 1634, 1485, 1381, 1282, 1153, 1106, 1058, 994, 953, 896, 818, 796, 769, 733, 645, 560, 523, 457, 374, 360, 336.

Synthesis of $\mathbf{I_{Cu}}$: $\mathbf{I_{Cu}}$ was synthesized through the same procedure as that for $\mathbf{I_{Ni}}$ using $Cu(OAc)_2\cdot 2H_2O$ (6.2 mg, 30.9 μmol) as the metal source (pale blue crystals, 47% yield based on Cu). Elemental analysis, calcd (%) for $C_{114}H_{270}Cl_2GaN_7O_{70}Si_2W_{18}$ ($TBA_7H_{11}[Cu(A\text{-}\alpha\text{-}SiW_9O_{34})_2]\cdot 2H_2O\cdot C_2H_4Cl_2$): C, 21.42; H, 4.27; N, 1.53; Si, 0.88; Cu, 0.99; W, 51.77. Found: C, 21.70; H, 4.23; N, 1.49; Si, 0.91; Cu, 1.05; W, 54.80. Positive-ion MS (CSI, 1,2-dichloroethane): *m/z* 3310 (calcd. 3310) $[TBA_9HCu(SiW_9O_{31})(SiW_9O_{32})]^{2+}$, 6431 (calcd. 6431) $[TBA_8H_7Cu(SiW_9O_{33})_2]^{+}$. IR (KBr pellet, cm^{-1}): 1636, 1618, 1484, 1473, 1381, 1153, 1107, 1059, 1005, 955, 915, 898, 817, 793, 765, 738, 718, 647, 563, 521, 457, 408, 377, 350, 339, 322, 269.

Synthesis of $\mathbf{I_{Ga}}$: $\mathbf{I_{Ga}}$ was synthesized through the same procedure as that for $\mathbf{I_{Ni}}$ using $Ga(acac)_3$ (11.3 mg, 30.9 μmol) as the metal source (colourless crystals, 49% yield based on Ga). Elemental analysis, calcd (%) for $C_{114}H_{270}Cl_2GaN_7O_{70}Si_2W_{18}$ ($TBA_7H_{10}[Ga(A\text{-}\alpha\text{-}SiW_9O_{34})_2]\cdot 2H_2O\cdot C_2H_4Cl_2$): C, 21.51; H, 4.28; N, 1.54; Si, 0.88; Ga, 1.10; W, 51.99. Found: C, 21.36; H, 4.32; N, 1.49; Si, 0.88; Ga, 1.11; W,

51.00. Positive-ion MS (CSI, 1,2-dichloroethane): *m/z* 3340 (calcd. 3340) $[TBA_9H_6Ga(SiW_9O_{33})_2]^{2+}$, 6437 (calcd. 6437) $[TBA_8H_6Ga(SiW_9O_{33})_2]^{+}$. IR (KBr pellet, cm^{-1}): 2962, 2934, 2874, 1635, 1485, 1382, 1153, 1108, 1066, 992, 955, 895, 816, 774, 738, 671, 560, 536, 511, 375, 360, 337.

The formations of II_{MMn4} from I_M can be expressed by Eq S2.

$TBA_7H_m[M(A\text{-}\alpha\text{-}SiW_9O_{34})_2]$ (**I_M**) + $4Mn(acac)_3$ + $2H_2O$

$\rightarrow$ $TBA_7H_n[MMn_4(OH)_2(A\text{-}\alpha\text{-}SiW_9O_{34})_2]$ (**II_{MMn4}**) + 12Hacac (Eq S2)

(M = Fe(III), Ga(III), n = 0, m = 10; M = Co(II), Ni(II), Cu(II), n = 1, m = 11)

Synthesis of II_{FeMn4}: To a 1,2-dichloroethane solution (12 mL) of **I_{Fe}** ($TBA_7H_{10}[Fe(A\text{-}\alpha\text{-}SiW_9O_{34})_2]\cdot 2H_2O\cdot C_2H_4Cl_2$; 254 mg, 40 μmol), $Mn(acac)_3$ (56 mg, 160 μmol, 4 equiv. with respect to **I_{Fe}**) was added, and the resulting solution was stirred for 6 h at room temperature (ca. 20°C). Then, diethyl ether (40 mL) was added. Dark brown precipitates formed were filtered off, followed by recrystallization from a mixed solvent of 1,2-dichloroethane and diethyl ether. The brown crystals of **II_{FeMn4}** suitable for X-ray crystallographic analysis were obtained (202 mg, 77% yield based on **I_{Fe}**). Elemental analysis, calcd (%) for $C_{114}H_{271}Cl_2CoN_7O_{70}Si_2W_{18}$ ($TBA_7H_2[FeMn_4O_2(A\text{-}\alpha\text{-}SiW_9O_{34})_2]\cdot 2H_2O\cdot C_2H_4Cl_2$): C, 20.76; H, 4.00; N, 1.49; Si, 0.85; Mn, 3.33; Fe 0.85; W, 50.18. Found: C, 20.71; H, 4.00; N, 1.51; Si, 0.84; Mn 3.35; Fe, 0.84; W, 50.46. Positive-ion MS (CSI, 1,2-dichloroethane): *m/z* 3473 (calcd. 3473) $[TBA_9H_2FeMn_4O_2(SiW_9O_{34})_2]^{2+}$, 6703 (calcd. 6703) $[TBA_8H_2FeMn_4O_2(SiW_9O_{34})_2]^{+}$. IR (KBr pellet, cm^{-1}): 1635, 1483, 1384, 1157, 1113, 1057, 1015, 957, 935, 923, 889, 875, 786, 712, 641, 532, 376, 335, 303, 289, 278, 267, 256.

Synthesis of II_{CoMn4}: II_{CoMn4} was synthesized through the same procedure as that for **II_{FeMn4}** using **I_{Co}** ($TBA_7H_{11}[Co(A\text{-}\alpha\text{-}SiW_9O_{34})_2]\cdot 2H_2O\cdot C_2H_4Cl_2$) as the starting material (dark brown crystals, 86% yield based on **I_{Co}**). Elemental analysis, calcd (%) for $C_{114}H_{272}Cl_2CoN_7O_{70}Si_2W_{18}$ ($TBA_7H_3[CoMn_4O_2(A\text{-}\alpha\text{-}SiW_9O_{34})_2]\cdot 2H_2O\cdot C_2H_4Cl_2$): C, 20.76; H, 4.00; N, 1.49; Si, 0.85; Mn 3.33; Co, 0.89; W, 50.14. Found: C, 20.51; H, 4.00; N, 1.49; Si, 0.79; Mn, 3.30; Co 0.88; W, 50.67. Positive-ion MS (CSI, 1,2-dichloroethane): *m/z* 3475 (calcd. 3475) $[TBA_9H_3CoMn_4O_2(SiW_9O_{34})_2]^{2+}$, 6707 (calcd. 6707) $[TBA_8H_3CoMn_4O_2(SiW_9O_{34})_2]^{+}$. IR (KBr pellet, cm^{-1}): 1635, 1484, 1381, 1152, 1107, 1061, 1008, 992, 957, 920, 894, 873, 788, 747, 700, 665, 537, 376, 329, 282, 278, 263, 255.

Synthesis of II_{NiMn4}: II_{NiMn4} was synthesized through the same procedure as that for **II_{FeMn4}** using **I_{Ni}** as the starting material (dark brown crystals, 71% yield based on **I_{Ni}**). Elemental analysis, calcd (%) for $C_{114}H_{263}Cl_2Mn_4N_7NiO_{72}Si_2W_{18}$ ($TBA_7H_3[NiMn_4O_2(A\text{-}\alpha\text{-}SiW_9O_{34})_2]\cdot 2H_2O\cdot C_2H_4Cl_2$): C, 20.76; H, 4.00;

N, 1.49; Si, 0.85; Mn 3.33; Ni, 0.89; W, 50.15. Found: C, 20.75; H, 4.04; N, 1.47; Si, 0.83; Mn 3.19; Ni, 0.85; W, 50.98. Positive-ion MS (CSI, 1,2-dichloroethane): *m/z* 3474 (calcd. 3474) $[TBA_9H_3NiMn_4O_2(SiW_9O_{34})_2]^{2+}$, 6706 (calcd. 6706) $[TBA_8H_3NiMn_4O_2(SiW_9O_{34})_2]^{+}$. IR (KBr pellet, cm^{-1}): 1634, 1484, 1382, 1152, 1105, 1065, 1009, 989, 957, 919, 891, 874, 788, 745, 668, 534, 480, 425, 379, 332, 286, 279, 269, 256, 252.

Synthesis of II_{CuMn4}: II_{CuMn4} was synthesized through the same procedure as that for **II_{FeMn4}** using **I_{Cu}** as the starting material (brown crystals, 86% yield based on **I_{Cu}**). $C_{114}H_{272}Cl_2CuN_7O_{70}Si_2W_{18}$ ($TBA_7H_3[CuMn_4O_2(A\text{-}\alpha\text{-}SiW_9O_{34})_2]\cdot 2H_2O\cdot C_2H_4Cl_2$): C, 20.73; H, 4.01; N, 1.48; Si, 0.85; Mn 3.33; Cu, 0.96; W, 50.11. Found: C, 20.60; H, 3.94; N, 1.41; Si, 0.84; Mn, 3.37; Cu 0.96; W, 49.73. Positive-ion MS (CSI, 1,2-dichloroethane): *m/z* 3477 (calcd. 3477) $[TBA_9H_3CuMn_4O_2(SiW_9O_{34})_2]^{2+}$, 6711 (calcd. 6711) $[TBA_8H_3CuMn_4O_2(SiW_9O_{34})_2]^{+}$. IR (KBr pellet, cm^{-1}): 1635, 1484, 1384, 1152, 1107, 1062, 1008, 957, 922, 903, 872, 786, 743, 661, 533, 373, 333, 297, 283, 277, 257.

Synthesis of II_{GaMn4}: II_{GaMn4} was synthesized through the same procedure as that for **II_{FeMn4}** using **I_{Ga}** as the starting material. The dark brown crystals of **II_{GaMn4}** suitable for X-ray crystallographic analysis were obtained by recrystallization of crude crystals from a mixed solvent of nitromethane and diethyl ether (43% yield based on **I_{Ga}**). Elemental analysis, calcd (%) for $C_{114}H_{262}Cl_2GaMn_4N_7O_{72}Si_2W_{18}$ ($TBA_7H_2[GaMn_4O_2(A\text{-}\alpha\text{-}SiW_9O_{34})_2]\cdot 2H_2O\cdot C_2H_4Cl_2$): C, 20.72; H, 4.00; N, 1.48; Si, 0.85; Mn, 3.33; Ga, 1.05; W, 50.07. Found: C, 20.57; H, 3.97; N, 1.45; Si, 0.85; Mn 3.01; Ga, 1.04; W, 51.12. Positive-ion MS (CSI, 1,2-dichloroethane): *m/z* 3479 (calcd. 3479) $[TBA_9H_2GaMn_4O_2(SiW_9O_{34})_2]^{2+}$, 6717 (calcd. 6717) $[TBA_8H_2GaMn_4O_2(SiW_9O_{34})_2]^{+}$. IR (KBr pellet, cm^{-1}): 1635, 1483, 1380, 1152, 1107, 1054, 1016, 987, 957, 935, 925, 893, 786, 710, 646, 551, 533, 410, 375, 335, 308, 254.

Table S1. Selected BVS values for **Mn5**, $\mathbf{II}_{\mathbf{FeMn4}}$, $\mathbf{II}_{\mathbf{CoMn4}}$, $\mathbf{II}_{\mathbf{NiMn4}}$, $\mathbf{II}_{\mathbf{CuMn4}}$, and $\mathbf{II}_{\mathbf{GaMn4}}$[a]

Mn5		$\mathbf{II}_{\mathbf{FeMn4}}$		$\mathbf{II}_{\mathbf{CoMn4}}$	$\mathbf{II}_{\mathbf{NiMn4}}$	$\mathbf{II}_{\mathbf{CuMn4}}$	$\mathbf{II}_{\mathbf{GaMn4}}$
W1	6.32	W1	6.12	6.16	6.12	6.07	6.11
W2	6.19	W2	6.17	6.09	6.06	6.10	6.13
W3	6.17	W3	6.15	6.08	6.01	6.03	6.08
W4	6.19	W4	6.09	6.08	6.13	6.12	6.06
W5	6.10	W5	6.01	6.12	6.14	6.02	6.10
W6	6.16	W6	6.04	6.09	6.09	5.98	6.07
W7	6.05	W7	6.14	6.18	6.20	6.06	6.11
W8	6.18	W8	6.16	6.16	6.15	5.94	6.10
W9	6.09	W9	6.09	6.11	6.11	6.10	6.04
W10	6.33	W10	6.16	6.12	6.14	6.15	6.10
W11	6.18	W11	6.09	6.11	6.12	6.06	6.09
W12	6.17	W12	6.06	6.13	6.09	5.98	6.12
W13	6.04	W13	6.09	6.13	6.14	6.05	6.04
W14	6.11	W14	6.14	6.09	6.11	6.10	6.11
W15	6.00	W15	6.14	5.99	6.07	6.04	6.05
W16	6.16	W16	6.18	6.14	6.17	6.00	6.10
W17	6.16	W17	6.17	6.11	6.19	6.01	6.16
W18	6.15	W18	6.15	6.13	6.12	6.05	6.14
Si1	4.06	Si1	3.99	4.01	3.95	3.90	3.97
Si2	4.00	Si2	3.99	3.96	3.99	3.95	3.96
Mn1	3.09	M1	3.05	2.13	2.03	2.12	3.07
Mn2	2.93	Mn1	2.99	3.08	3.01	2.96	2.94
Mn3	2.90	Mn2	3.01	2.98	2.97	2.88	2.95
Mn4	2.92	Mn3	3.02	3.02	3.09	3.01	2.99
Mn5	2.92	Mn4	2.99	2.98	2.99	2.95	2.98
O1H	1.14	O1H	1.16	1.17	1.19	1.18	1.16
O2H	1.14	O2H	1.17	1.18	1.16	1.17	1.15
O3	1.78	O3	1.88	1.81	1.21	1.22	1.88
O40	1.73	O40	1.86	1.20	1.80	1.81	1.92

[a] M = Fe ($\mathbf{II}_{\mathbf{FeMn4}}$), Co ($\mathbf{II}_{\mathbf{CoMn4}}$), Ni ($\mathbf{II}_{\mathbf{NiMn4}}$), Cu ($\mathbf{II}_{\mathbf{CuMn4}}$), and Ga ($\mathbf{II}_{\mathbf{GaMn4}}$).

Table S2. Selected bond lengths and angles for **Mn5**, **II$_{FeMn4}$**, **II$_{CoMn4}$**, **II$_{NiMn4}$**, **II$_{CuMn4}$**, and **II$_{GaMn4}$**[a]

Bond length (Å)							
	Mn5		**II$_{FeMn4}$**	**II$_{CoMn4}$**	**II$_{NiMn4}$**	**II$_{CuMn4}$**	**II$_{GaMn4}$**
Mn1···Mn$_{avg}$	**3.457**	**M1···Mn$_{avg}$**	**3.514**	**3.488**	**3.492**	**3.461**	**3.509**
Mn1···Mn2	3.448	M1···Mn1	3.505	3.481	3.466	3.468	3.511
Mn1···Mn3	3.437	M1···Mn2	3.524	3.464	3.495	3.432	3.505
Mn1···Mn4	3.464	M1···Mn3	3.522	3.512	3.501	3.476	3.500
Mn1···Mn5	3.477	M1···Mn4	3.503	3.493	3.506	3.469	3.518
Mn2···Mn3	3.492	Mn1···Mn2	3.538	3.501	3.499	3.492	3.530
Mn4···Mn5	3.509	Mn3···Mn4	3.524	3.531	3.530	3.517	3.533
Mn2···Mn5	5.969	Mn1···Mn4	6.088	6.031	6.029	5.979	6.079
Mn3···Mn4	5.952	Mn2···Mn3	6.061	6.018	6.042	5.960	6.048
Mn1–O$_{avg}$	**2.019**	**M1–O$_{avg}$**	**2.010**	**2.080**	**2.057**	**2.079**	**1.980**
Mn1–O1	1.935	M1–O1	1.988	2.034	2.020	2.017	1.944
Mn1–O2	1.947	M1–O2	1.973	2.029	2.031	2.000	1.959
Mn1–O35	1.945	M1–O35	1.983	2.061	2.039	2.003	1.946
Mn1–O36	1.948	M1–O36	2.002	2.043	2.038	1.985	1.961
Mn1–O19	2.175	M1–O19	2.061	2.151	2.105	2.239	2.033
Mn1–O53	2.163	M1–O53	2.055	2.163	2.110	2.231	2.038
Mn–OH$_{avg}$	**1.968**	**Mn–OH$_{avg}$**	**1.961**	**1.957**	**1.957**	**1.956**	**1.963**
Mn2–O1H	1.981	Mn1–O1H	1.963	1.961	1.953	1.953	1.972
Mn3–O1H	1.954	Mn2–O1H	1.956	1.949	1.954	1.956	1.958
Mn4–O2H	1.970	Mn3–O2H	1.961	1.962	1.963	1.963	1.962
Mn5–O2H	1.966	Mn4–O2H	1.965	1.957	1.957	1.952	1.959
Mn–O$_{Siavg}$	**2.196**	**Mn–O$_{Siavg}$**	**2.154**	**2.155**	**2.150**	**1.948**	**2.146**
Mn1–O20	2.202	Mn1–O(Si)	2.152	2.163	2.155	2.191	2.143
Mn2–O21	2.196	Mn2–O(Si)	2.162	2.163	2.166	2.180	2.144
Mn3–O54	2.183	Mn3–O(Si)	2.155	2.137	2.151	2.152	2.151
Mn4–O55	2.203	Mn4–O(Si)	2.147	2.157	2.129	2.170	2.147
Bond Angle (°)							
	Mn5		**II$_{FeMn4}$**	**II$_{CoMn4}$**	**II$_{NiMn4}$**	**II$_{CuMn4}$**	**II$_{GaMn4}$**
θ_{1avg}	**128.61**	**θ_{1avg}**	**129.49**	**125.62**	**126.43**	**125.30**	**130.25**
Mn1–O35–Mn2	128.14	M1–O35-Mn1	129.14	126.04	126.33	125.97	130.58
Mn1–O36–Mn3	129.57	M1–O36-Mn2	131.08	125.78	126.85	124.72	129.72
Mn1–O1–Mn4	129.24	M1–O1-Mn3	129.92	125.46	126.13	124.88	130.21
Mn1–O2–Mn5	127.47	M1–O2-Mn4	127.81	125.18	126.41	125.64	130.50
θ_{2avg}	**125.61**	**θ_{2avg}**	**128.32**	**127.85**	**127.81**	**127.20**	**128.20**
Mn2–O1H–Mn3	125.08	Mn1–O1H–Mn2	129.00	127.14	127.18	126.59	127.82
Mn4–O2H–Mn5	126.13	Mn3–O2H–Mn4	127.64	128.56	128.44	127.81	128.57

[a] M = Fe (**II$_{FeMn4}$**), Co (**II$_{CoMn4}$**), Ni (**II$_{NiMn4}$**), Cu (**II$_{CuMn4}$**), and Ga (**II$_{GaMn4}$**).

Table S3. The thermal energy barrier for magnetic relaxation (U_{eff}) and pre-exponential factor (τ_0) for **Mn5**, $\mathbf{II}_{\mathbf{FeMn4}}$, $\mathbf{II}_{\mathbf{CoMn4}}$, $\mathbf{II}_{\mathbf{NiMn4}}$, and $\mathbf{II}_{\mathbf{CuMn4}}$

	U_{eff} / K (/cm^{-1})	τ_0 / s
Mn5	19.5 (13.6)	1.5×10^{-8}
$\mathbf{II}_{\mathbf{FeMn4}}$	31.4 (22.0)	1.6×10^{-8}
$\mathbf{II}_{\mathbf{CoMn4}}$	22.3 (15.2)	3.4×10^{-8}
$\mathbf{II}_{\mathbf{NiMn4}}$	19.4 (13.5)	6.0×10^{-9}
$\mathbf{II}_{\mathbf{CuMn4}}$	23.1 (16.0)	1.4×10^{-8}

Table S4. The α values in Cole-Cole plots and the relaxation time (τ) of **Mn5** at each temperature

T / K	α	τ / s
1.85	0.16	0.000995
1.90	0.13	0.000796
2.00	0.10	0.000455
2.20	0.10	0.000187
2.40	0.06	0.000100

Table S5. The α values in Cole-Cole plots and the relaxation time (τ) of $\mathbf{II_{FeMn4}}$ at each temperature

T / K	α	τ / s
1.8	0.17	-
1.9	0.12	-
2.0	0.10	0.039789
2.2	0.06	0.014469
2.4	0.06	0.005684
2.6	0.05	0.002526
2.8	0.05	0.001224
3.0	0.05	0.000589
3.2	0.05	0.000319
3.4	0.05	0.000159

Table S6. The α values in Cole-Cole plots and the relaxation time (τ) of $\mathbf{II_{CoMn4}}$ at each temperature

T / K	α	τ / s
1.8	0.17	0.003979
1.9	0.14	0.002526
2.0	0.15	0.001768
2.2	0.16	0.000838
2.4	0.14	0.000379

Table S7. The α values in Cole-Cole plots and the relaxation time (τ) of $\mathbf{II_{NiMn4}}$ at each temperature

T / K	α	τ / s
1.8	0.28	0.000796
1.9	0.23	0.000455
2.0	0.20	0.000265
2.2	0.22	0.000199
2.4	0.22	0.000133
2.6	0.27	0.000106

Table S8. The α values in Cole-Cole plots and the relaxation time (τ) of $\mathbf{II_{CuMn4}}$ at each temperature

T / K	α	τ / s
1.8	0.17	0.602762
1.9	0.12	0.240662
2.0	0.10	0.039789
2.2	0.06	0.014469
2.4	0.06	0.005684

Table S9. Crystallographic data for $\mathbf{I_{Ni}}$, $\mathbf{I_{Cu}}$, and $\mathbf{I_{Ga}}$

Compound	$\mathbf{I_{Ni}}$	$\mathbf{I_{Cu}}$	$\mathbf{I_{Ga}}$
formula	$C_{124}Cl_{12}N_7NiO_{70}Si_2W_{18}$	$C_{124}Cl_{12}CuN_7O_{70}Si_2W_{18}$	$C_{124}Cl_{12}GaN_7O_{70}Si_2W_{18}$
Fw (g mol^{-1})	6556.9	6561.73	6567.91
crystal system	triclinic	triclinic	triclinic
space group	*P*-1 (#2)	*P*-1 (#2)	*P*-1 (#2)
a (Å)	14.65510(10)	14.62560(10)	14.6663(2)
b (Å)	18.7075(2)	18.7678(2)	18.6722(3)
c (Å)	19.0611(2)	19.1230(2)	19.0211(3)
α (deg)	106.8700(10)	107.2098(5)	106.6060(6)
β (deg)	92.2040(10)	92.3267(5)	92.4161(8)
γ (deg)	98.1760(10)	98.2091(6)	97.9290(10)
V (Å^3)	4932.51(8)	4943.60(8)	4925.69(14)
Z	1	1	1
temp (K)	123(2)	123(2)	123(2)
ρ_{calcd} (g cm^{-3})	2.207	2.204	2.214
GOF	1.046	1.107	1.041
R_1 [$I>2\sigma(I)$]	0.0687 (for 24370 data)	0.0624 (for 14890 data)	0.0794 (for 20971 data)
wR_2	0.1653 (for all 26720 data)	0.1406 (for all 15244 data)	0.2126 (for all 27152 data)

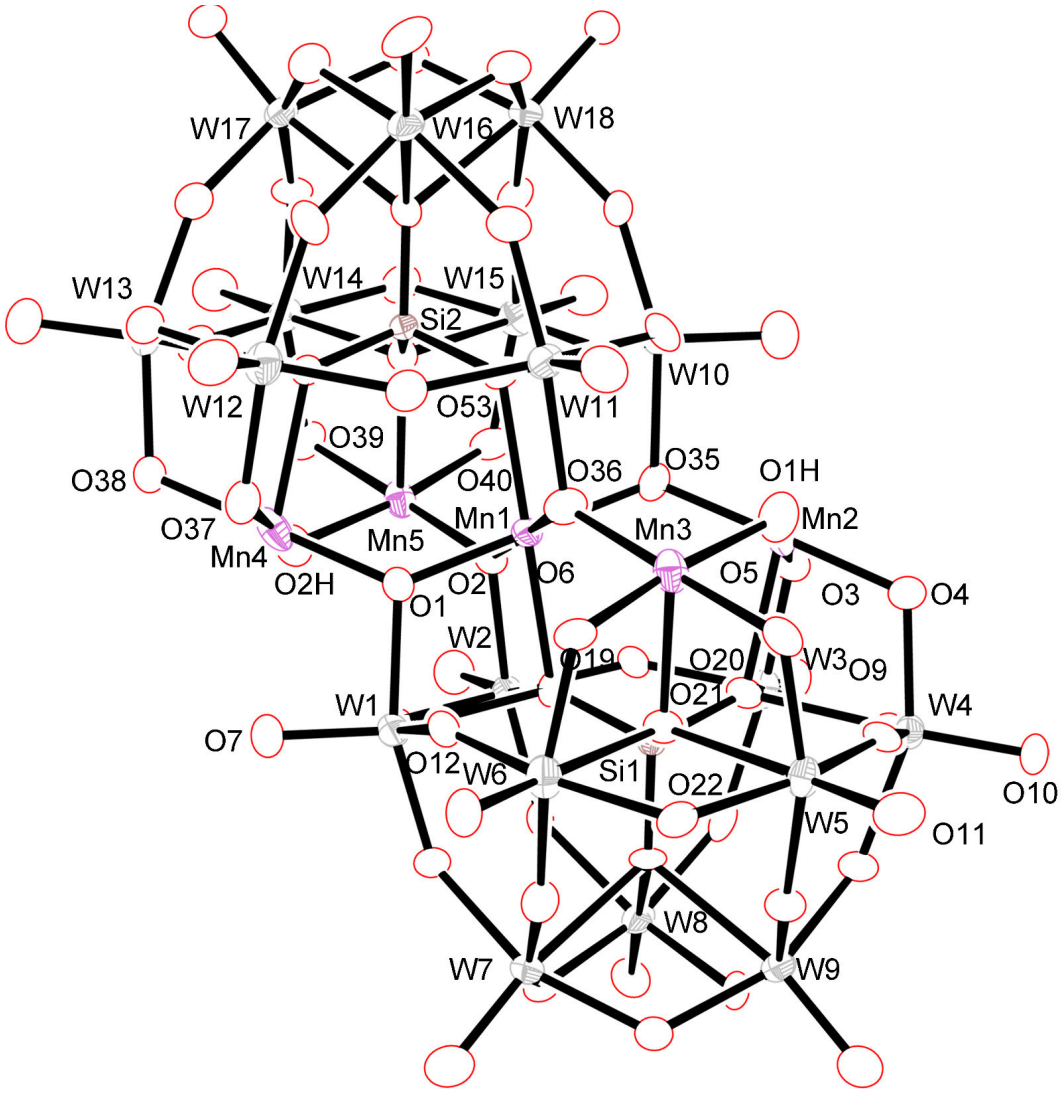

Fig. S1 ORTEP representation of the anion part of **Mn5** with thermal ellipsoids drawn at the 50% probability level.

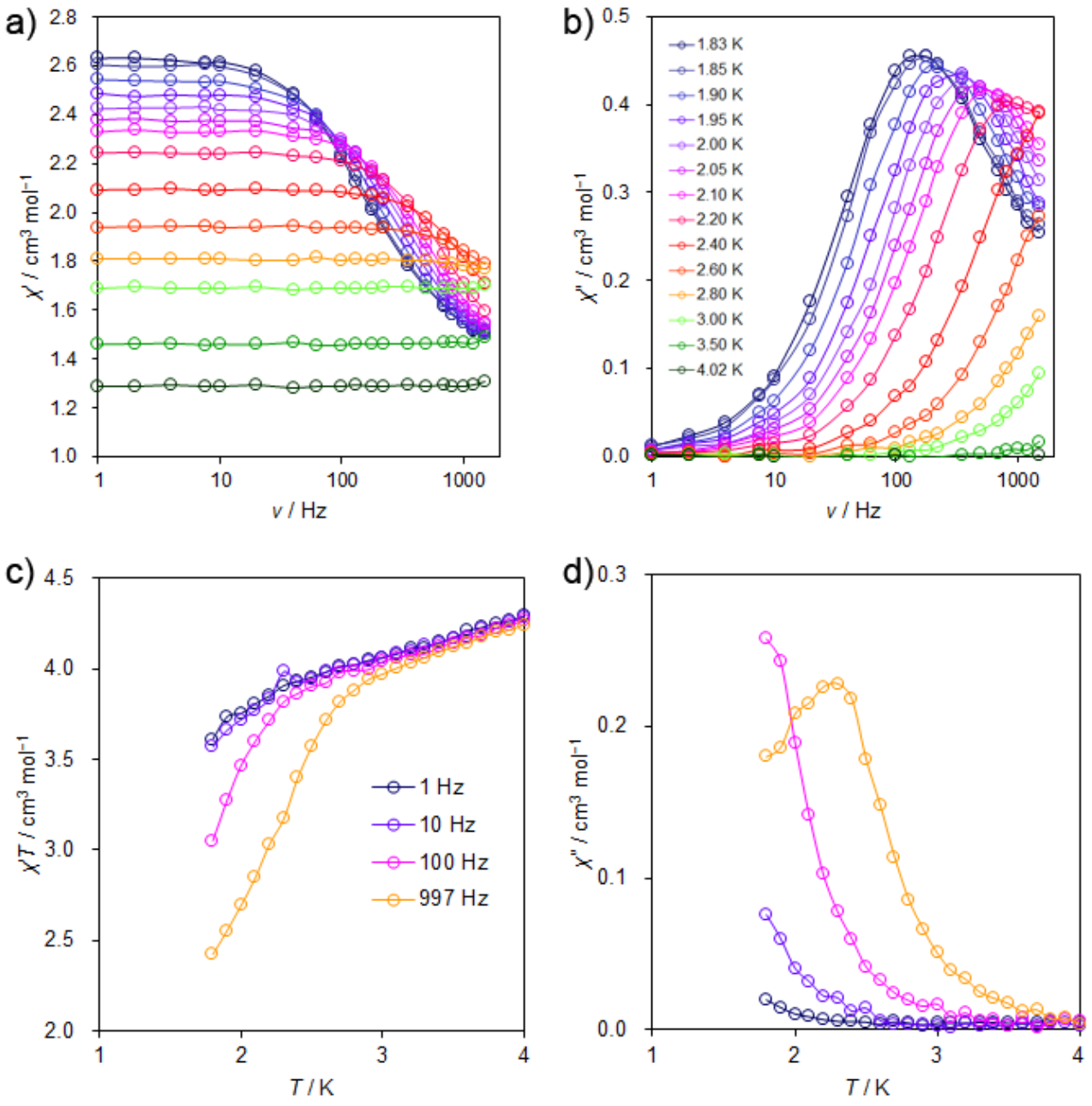

Fig. S2 Frequency dependence of the ac magnetic susceptibility ((a) χ' and (b) χ'') and temperature dependence of the ac magnetic susceptibility ((c) $\chi'T$ and (d) χ'') of **Mn5** under the zero external dc field.

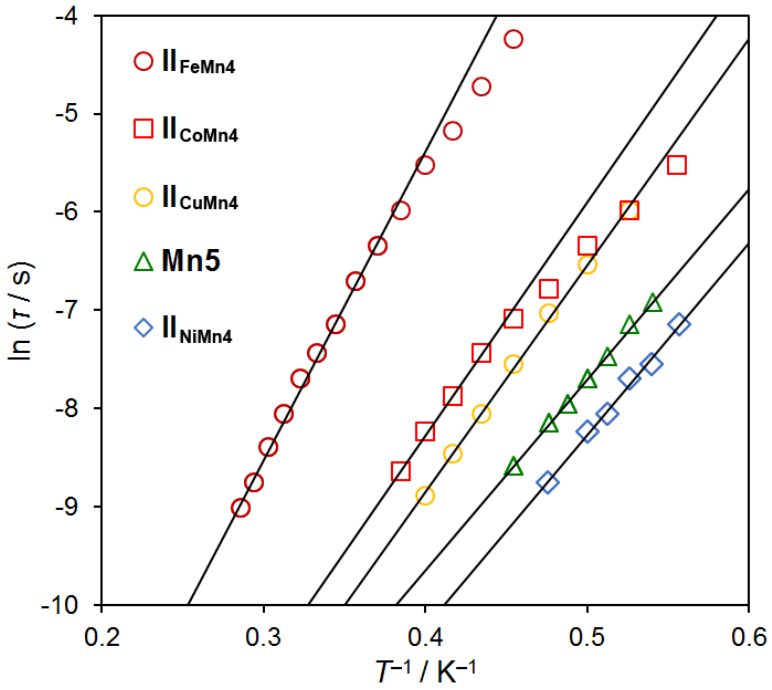

Fig. S3 Plots of relaxation time (τ) versus T^{-1} for **Mn5**, $\mathbf{II}_{\mathbf{FeMn4}}$, $\mathbf{II}_{\mathbf{CoMn4}}$, $\mathbf{II}_{\mathbf{NiMn4}}$, and $\mathbf{II}_{\mathbf{CuMn4}}$. The solid lines represent the best fit with the Arrhenius law ($\ln\tau$ ($\tau = \tau_0\exp(U_{\text{eff}}/k_{\text{B}}T)$) *vs* T^{-1}) at thermally activated regime.

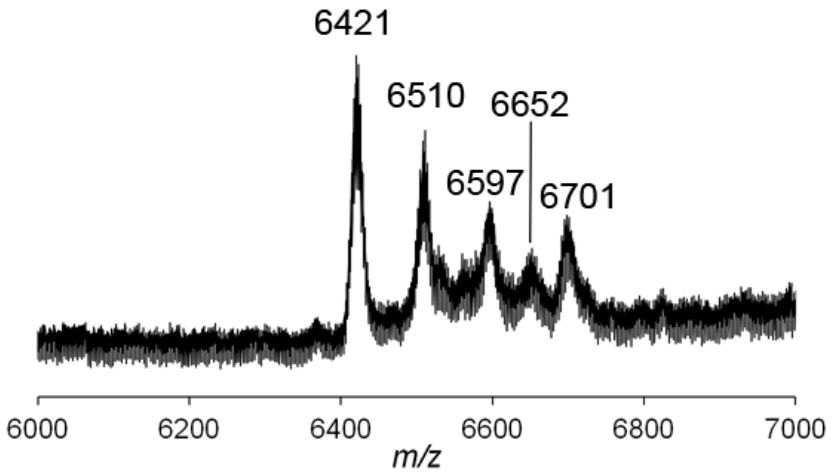

Fig. S4 Positive-ion CSI-mass spectrum of the reaction solution of $Ga(acac)_3$, $Mn(acac)_3$, and $TBA_4H_6[A\text{-}\alpha\text{-}SiW_9O_{34}]\cdot 2H_2O$ (1:4:2 molar ratio) in 1,2-dichloroethane. The sets of signals centred at *m/z* 6421, 6510, 6597, 6652, and 6701 were assignable to $[TBA_8H_6Mn(SiW_9O_{33})_2]^+$, $[TBA_8H_7Mn_2(SiW_9O_{34})_2]^+$, $[TBA_8H_8Mn_3O_2(SiW_9O_{34})_2]^+$, $[TBA_8H_5Mn_4O_2(SiW_9O_{34})_2]^+$, and $[TBA_8H_2Mn_5O_2(SiW_9O_{34})_2]^+$, respectively.

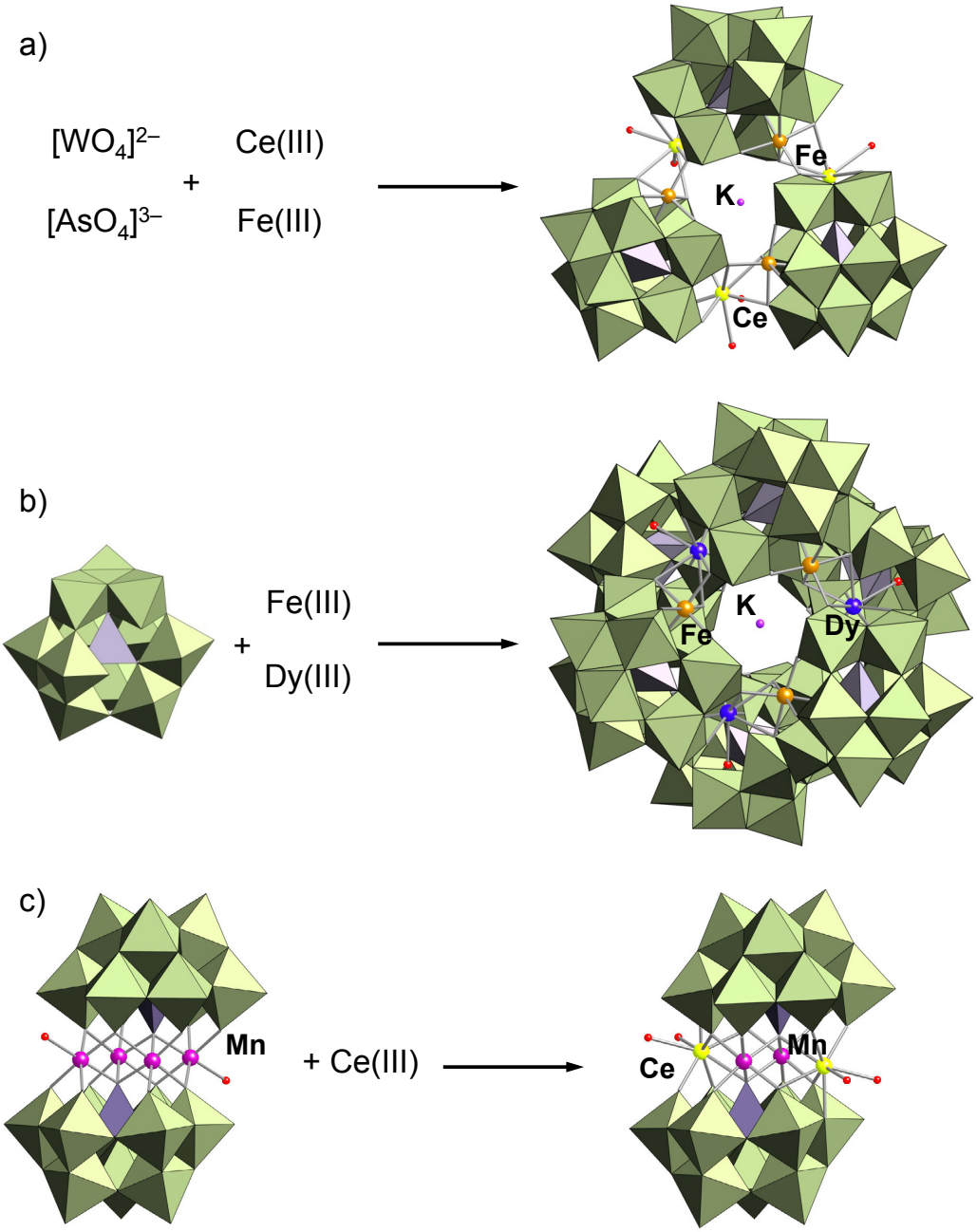

Fig. S5 Schematic representation of the reported synthetic methods for hetero-multinuclear metal-containing POMs. (a) The reaction of two types of metal cations with starting reagents (such as Na_2WO_4, Na_2HAsO_4),[12] (b) the reaction of two types of metal cations with lacunary POMs,[13] and (c) the exchange of the substituted metal cations in POMs with other metal cations.[14]

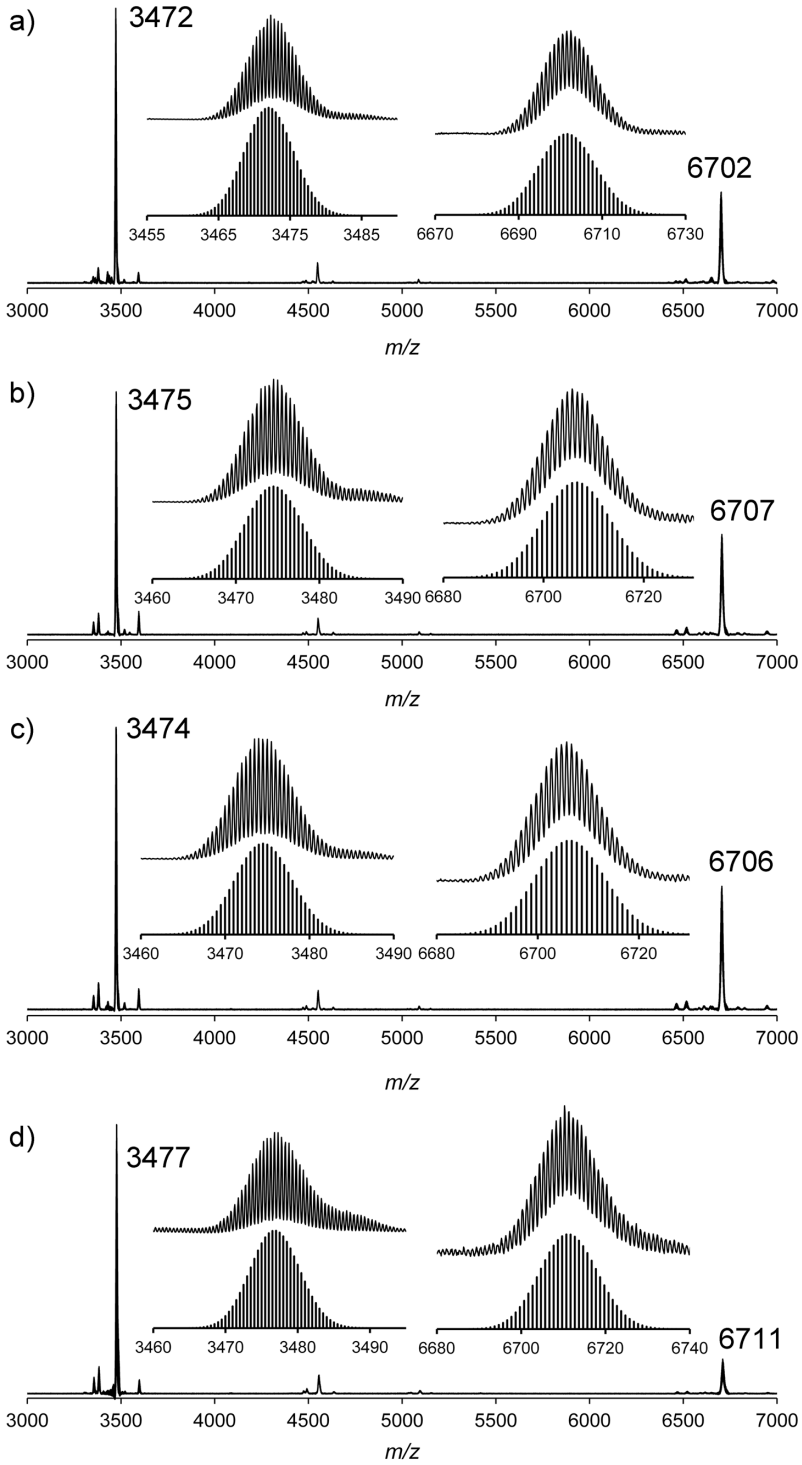

Fig. S6 Positive-ion CSI-mass spectra of (a) **Mn5**, (b) $\mathbf{II_{CoMn4}}$, (c) $\mathbf{II_{NiMn4}}$, and (d) $\mathbf{II_{CuMn4}}$ in 1,2-dichloroethane. Insets: (a) spectra in the range of *m/z* 3455–3490 and 6670–6730 and simulated patterns for $[TBA_9H_2Mn_5O_2(SiW_9O_{34})_2]^{2+}$ (*m/z* 3472) and $[TBA_8H_2Mn_5O_2(SiW_9O_{34})_2]^{+}$ (*m/z* 6702), (b) spectra in the range of *m/z* 3460–3490 and 6680–6730 and simulated patterns for $[TBA_9H_3CoMn_4O_2(SiW_9O_{34})_2]^{2+}$ (*m/z* 3475) and $[TBA_8H_3CoMn_4O_2(SiW_9O_{34})_2]^{+}$ (*m/z* 6707), (c) spectra in the range of *m/z* 3460–3490 and 6680–6730 and simulated patterns for $[TBA_9H_3NiMn_4O_2(SiW_9O_{34})_2]^{2+}$ (*m/z* 3474) and $[TBA_8H_3NiMn_4O_2(SiW_9O_{34})_2]^{+}$ (*m/z* 6706), (d) spectra in the range of *m/z* 3460–3495 and 6680–6740 and simulated patterns for $[TBA_9H_3CuMn_4O_2(SiW_9O_{34})_2]^{2+}$ (*m/z* 3477) and $[TBA_8H_3CuMn_4O_2(SiW_9O_{34})_2]^{+}$ (*m/z* 6711).

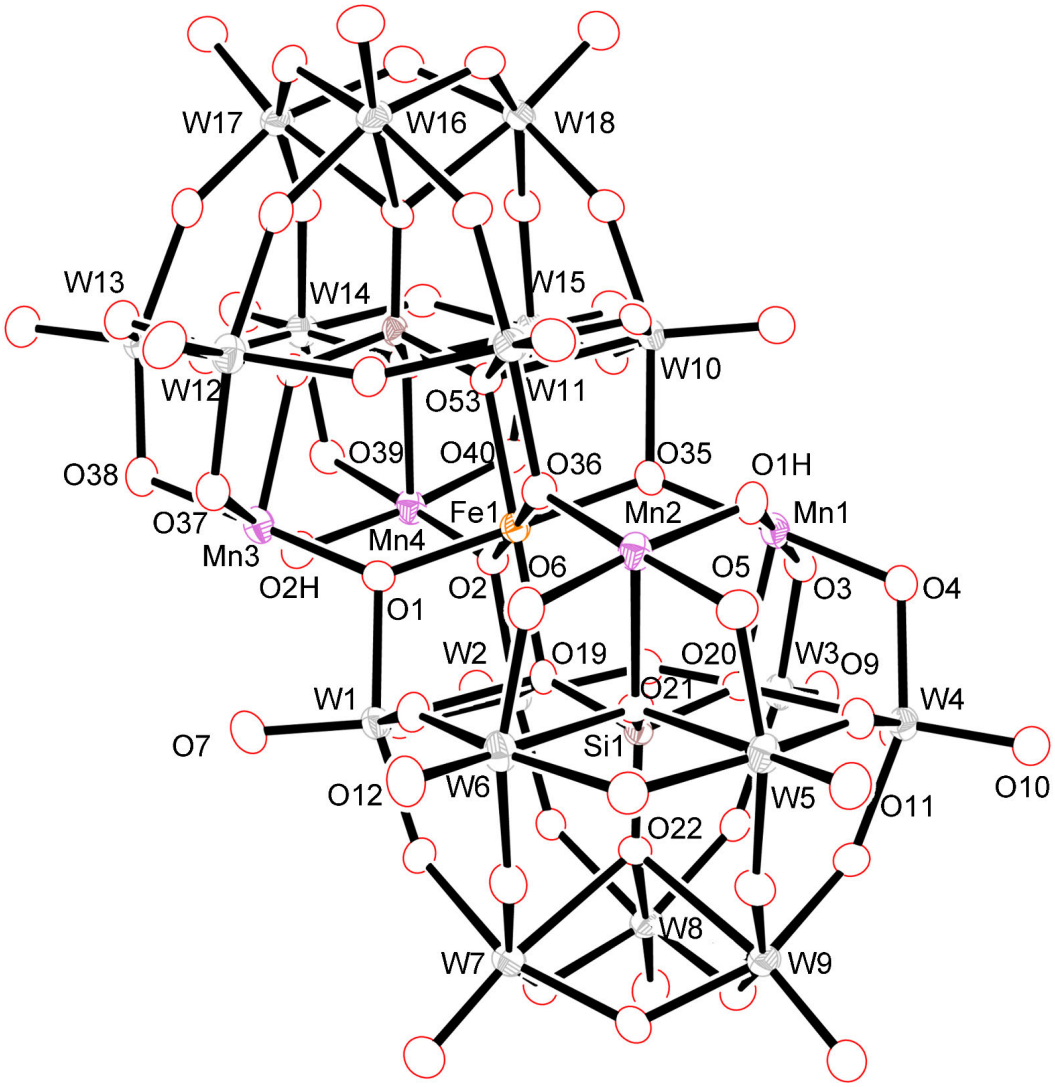

Fig. S7 ORTEP representation of the anion part of $\mathbf{II}_{\mathbf{FeMn4}}$ with thermal ellipsoids drawn at the 50% probability level.

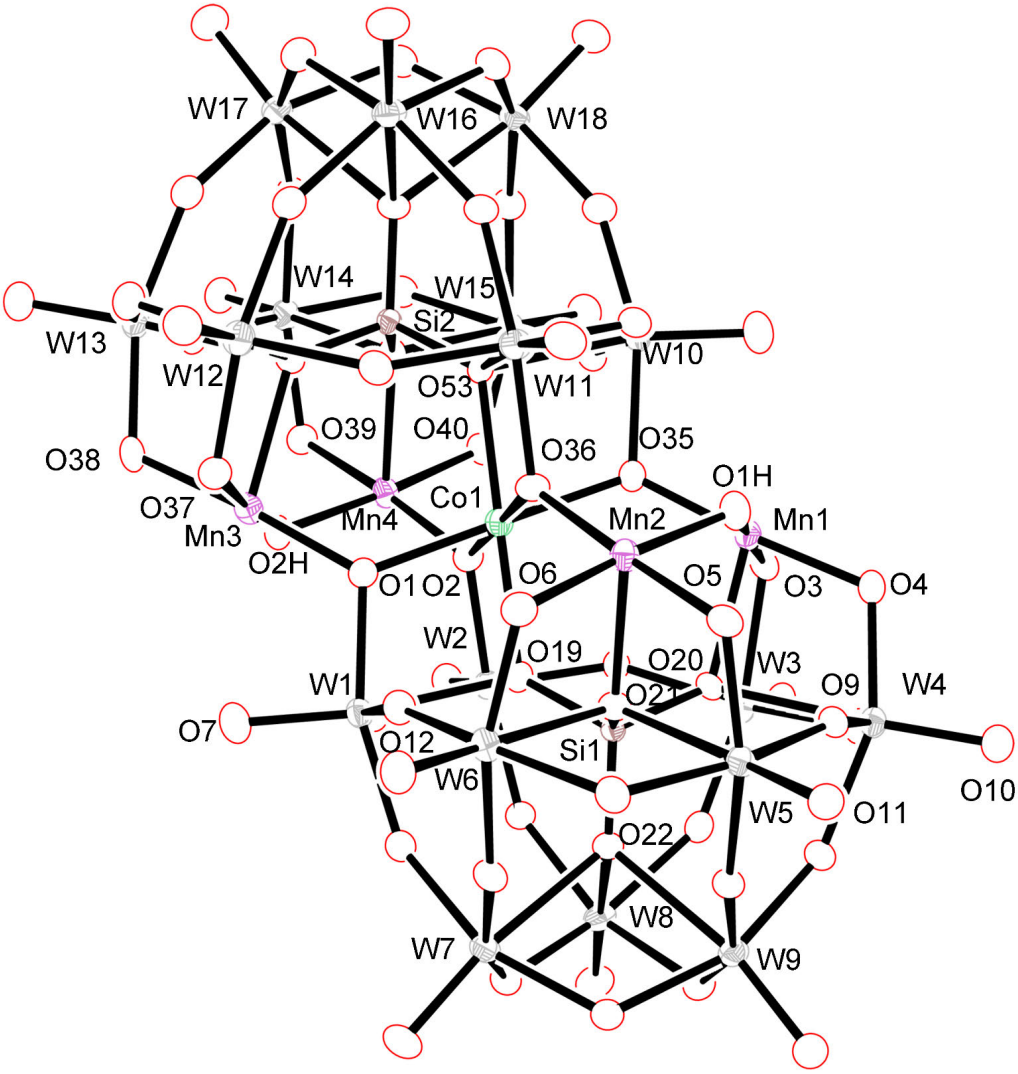

Fig. S8 ORTEP representation of the anion part of $\mathbf{II}_{\mathbf{CoMn4}}$ with thermal ellipsoids drawn at the 50% probability level.

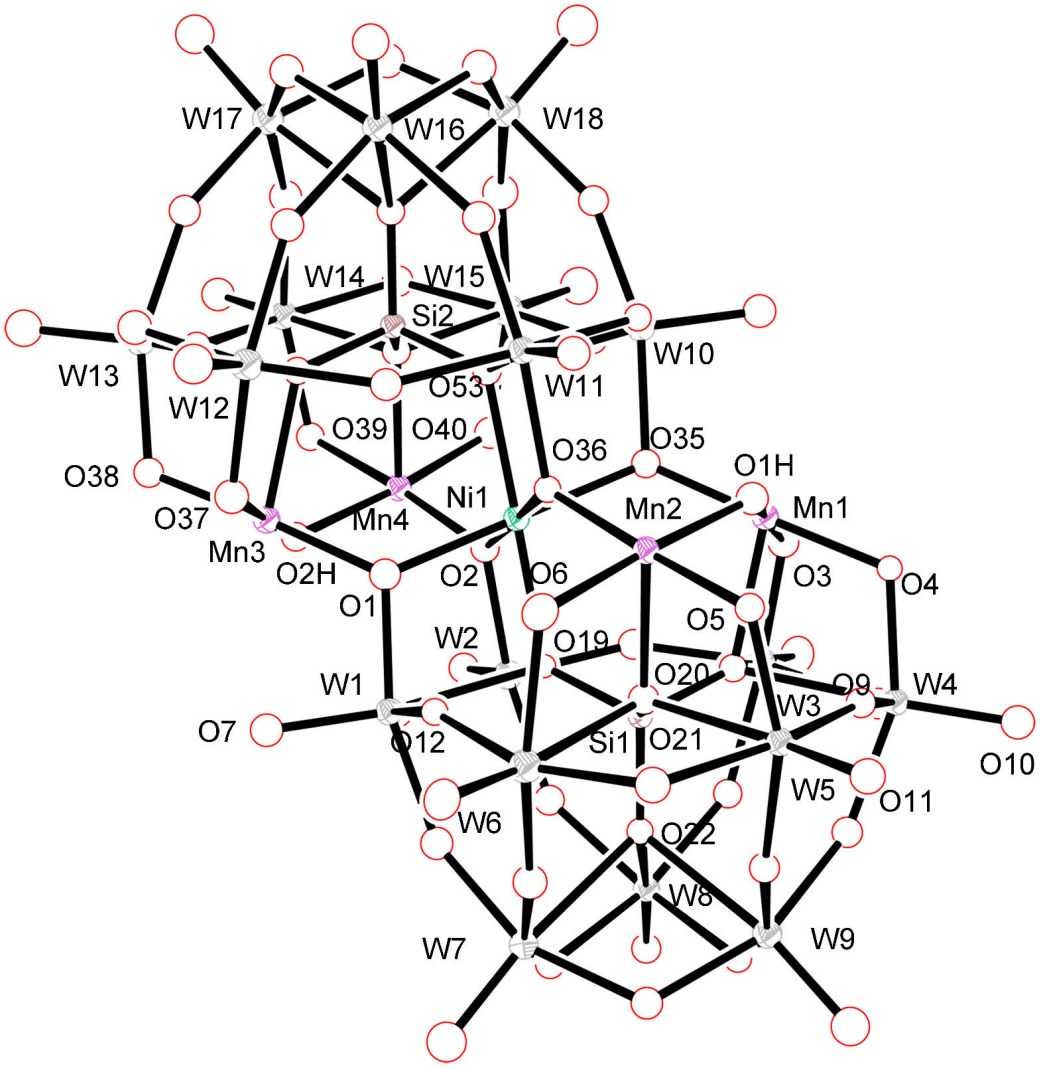

Fig. S9 ORTEP representation of the anion part of $\mathbf{II}_{\mathbf{NiMn4}}$ with thermal ellipsoids drawn at the 50% probability level.

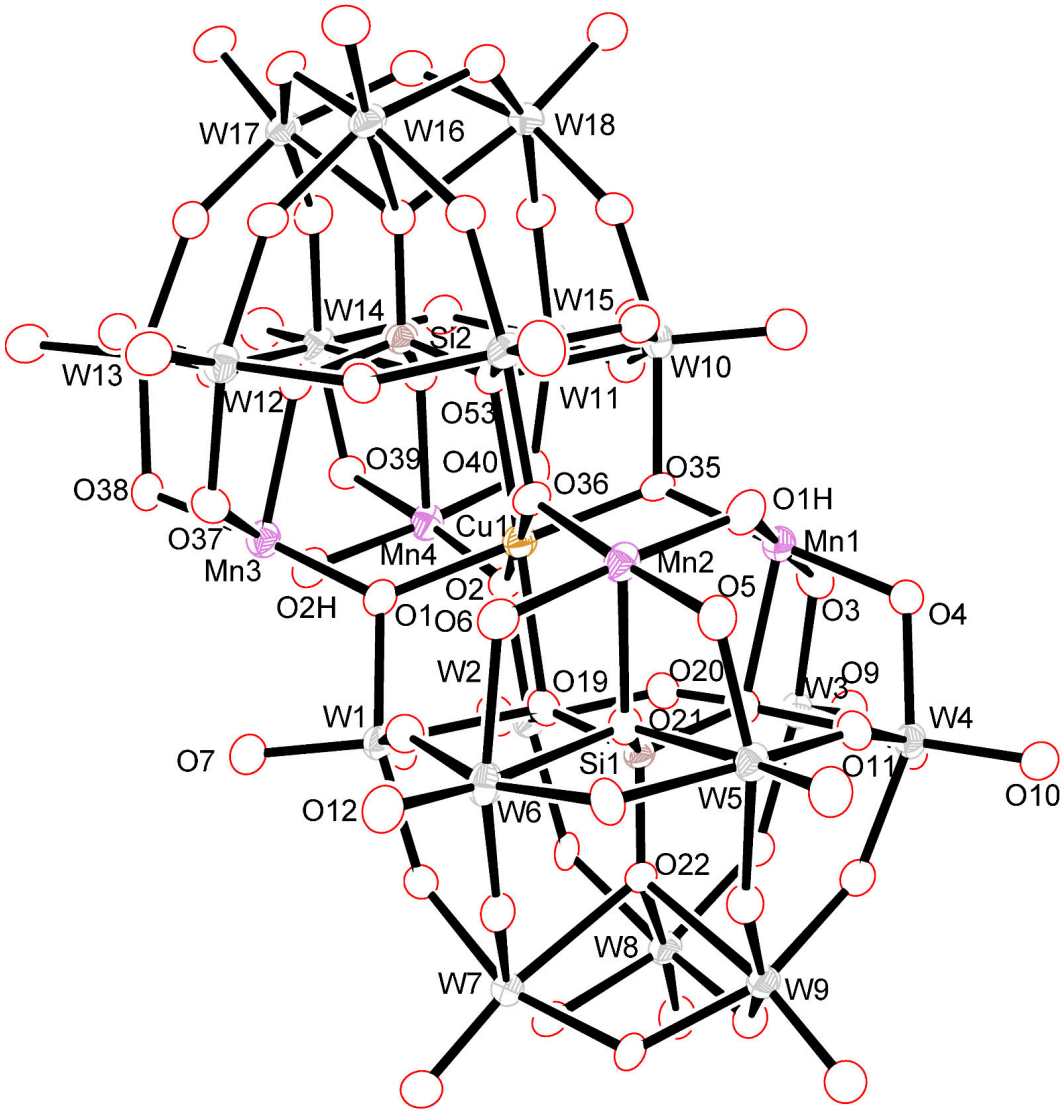

Fig. S10 ORTEP representation of the anion part of $\mathbf{II}_{\mathbf{CuMn4}}$ with thermal ellipsoids drawn at the 50% probability level.

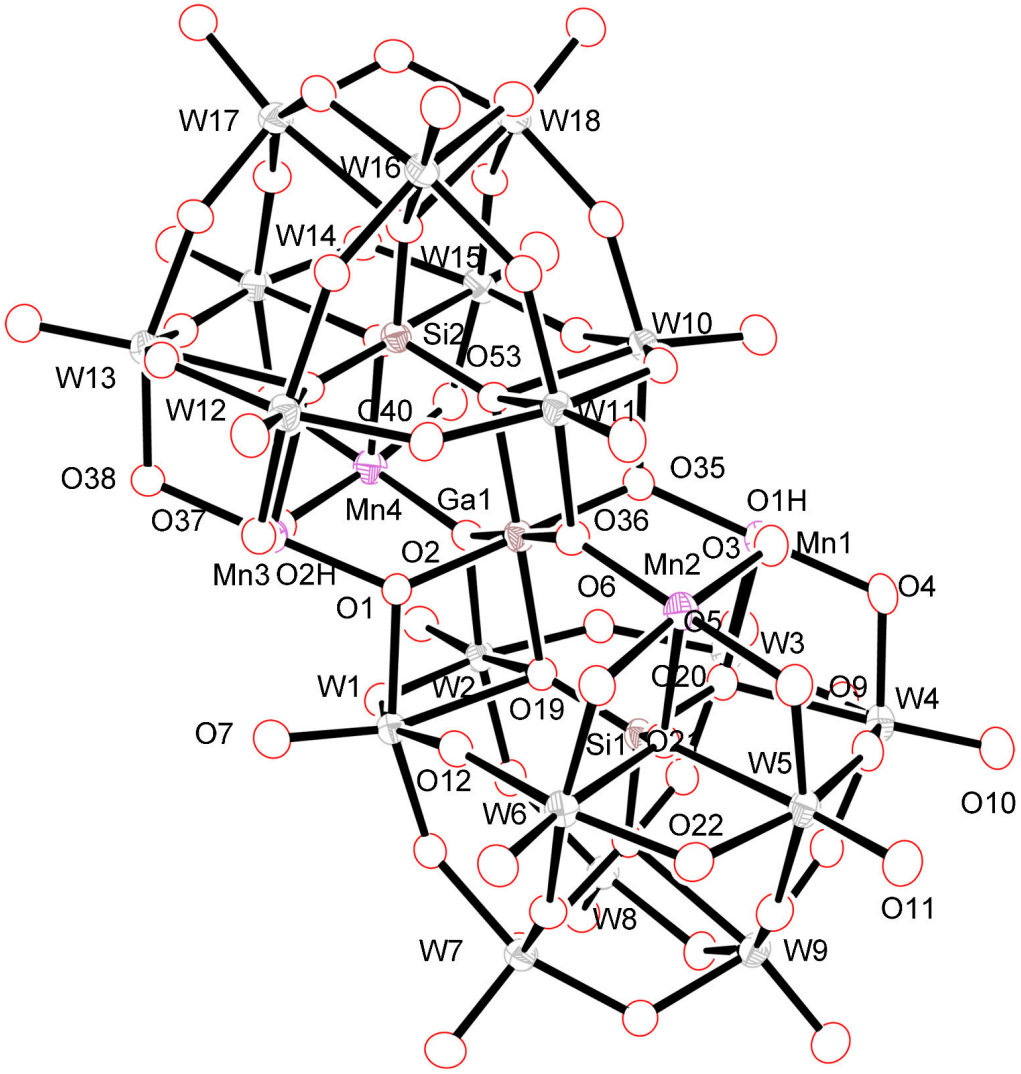

Fig. S11 ORTEP representation of the anion part of $\mathbf{II}_{\mathbf{GaMn4}}$ with thermal ellipsoids drawn at the 50% probability level.

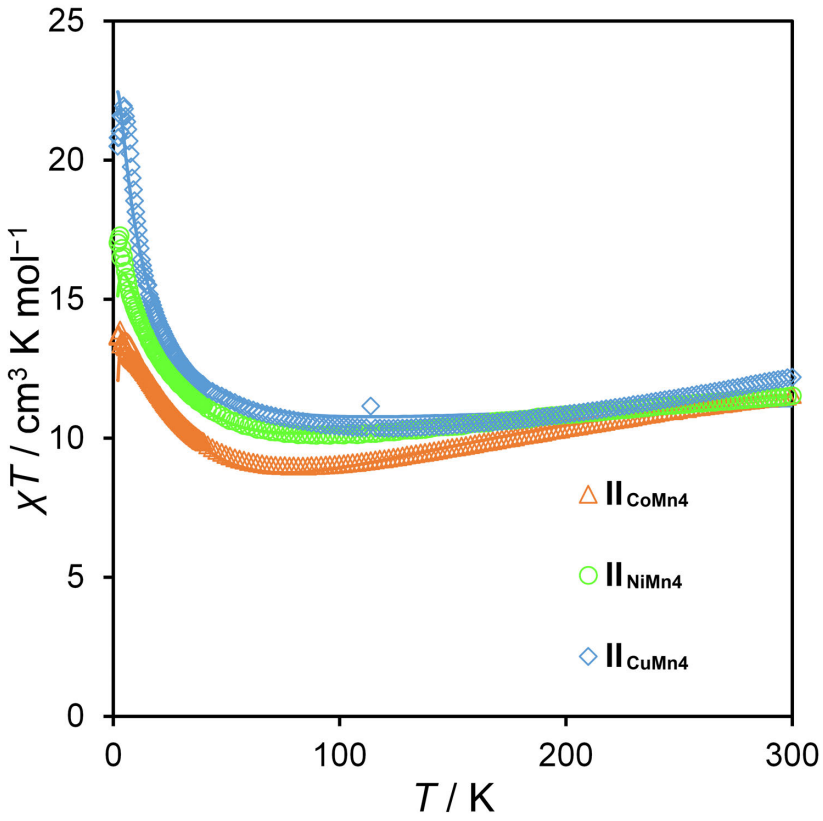

Fig. S12 Temperature dependence of χT for $\mathbf{II}_{\mathbf{CoMn4}}$, $\mathbf{II}_{\mathbf{NiMn4}}$, and $\mathbf{II}_{\mathbf{CuMn4}}$ under the applied field of 0.1 T. Solid lines represent the best fits.

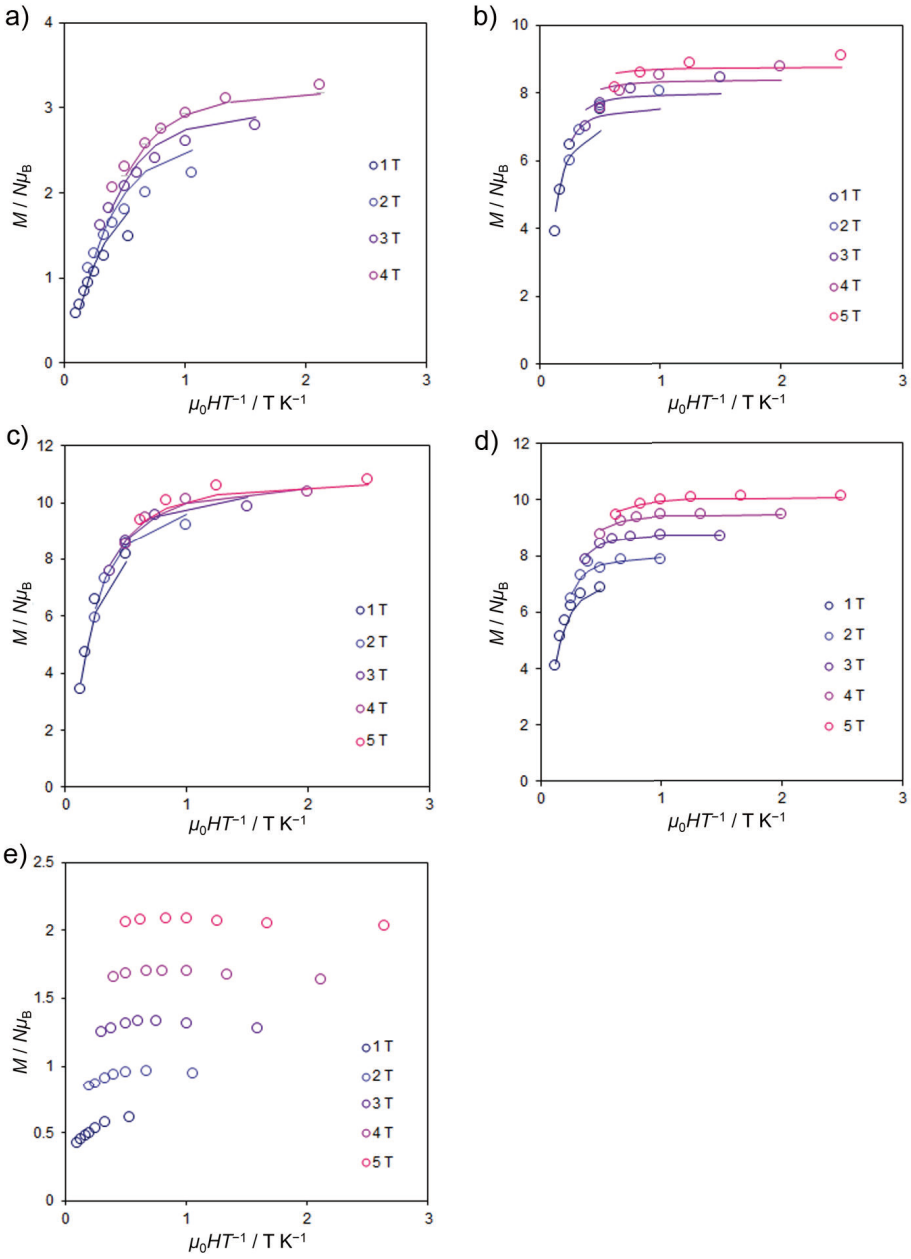

Fig. S13 Low temperature magnetization data for (a) **Mn5**, (b) $\mathbf{II}_{\mathbf{CoMn4}}$, (c) $\mathbf{II}_{\mathbf{NiMn4}}$, (d) $\mathbf{II}_{\mathbf{CuMn4}}$, and (e) $\mathbf{II}_{\mathbf{GaMn4}}$. Solid lines represent the best fits.

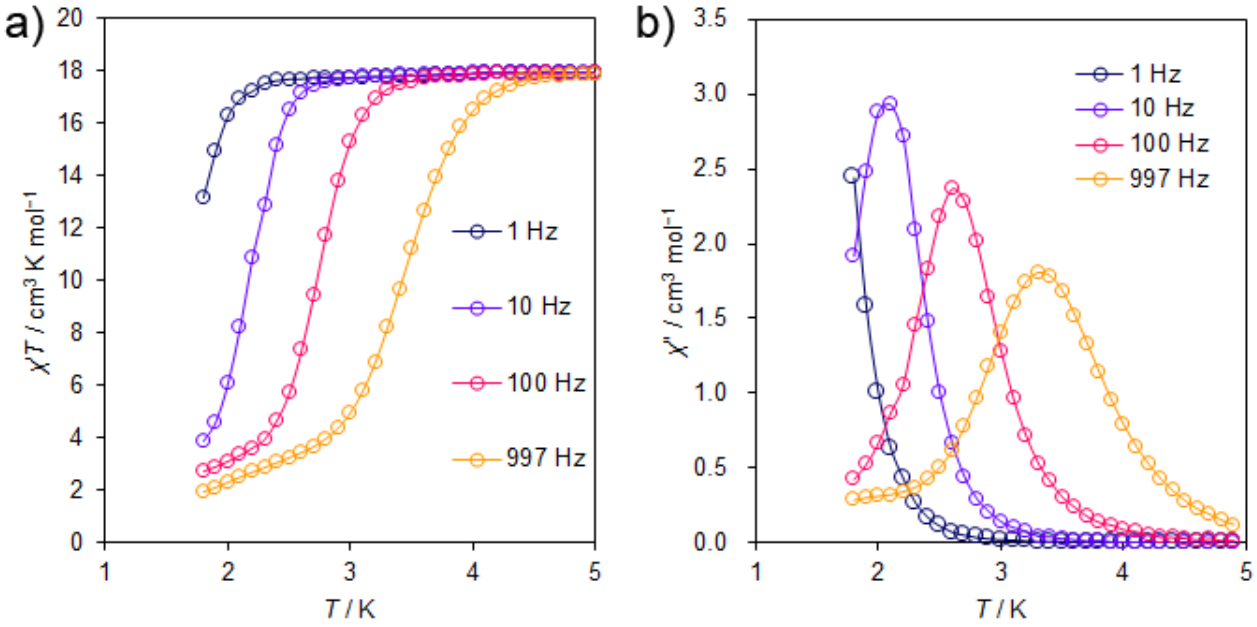

Fig. S14 Temperature dependence of the ac magnetic susceptibility $\chi'T$ and χ'' of $\mathbf{II}_{\mathbf{FeMn4}}$ under the zero external dc field.

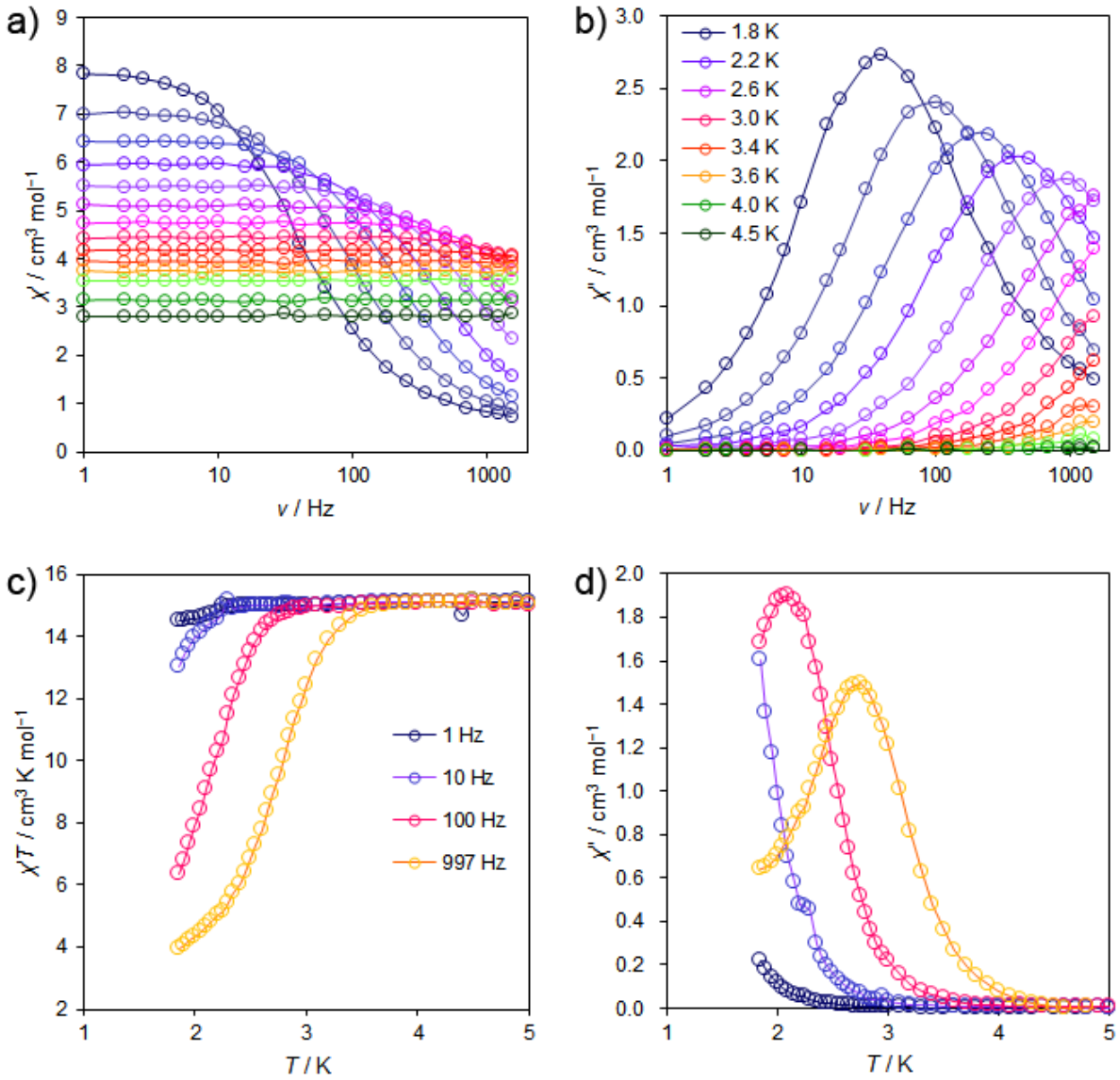

Fig. S15 Frequency dependence of the ac magnetic susceptibility ((a) χ' and (b) χ'') and temperature dependence of the acmagnetic susceptibility ((c) $\chi'T$ and (d) χ'') of $\mathbf{II}_{\mathbf{CoMn4}}$ under the zero external dc field.

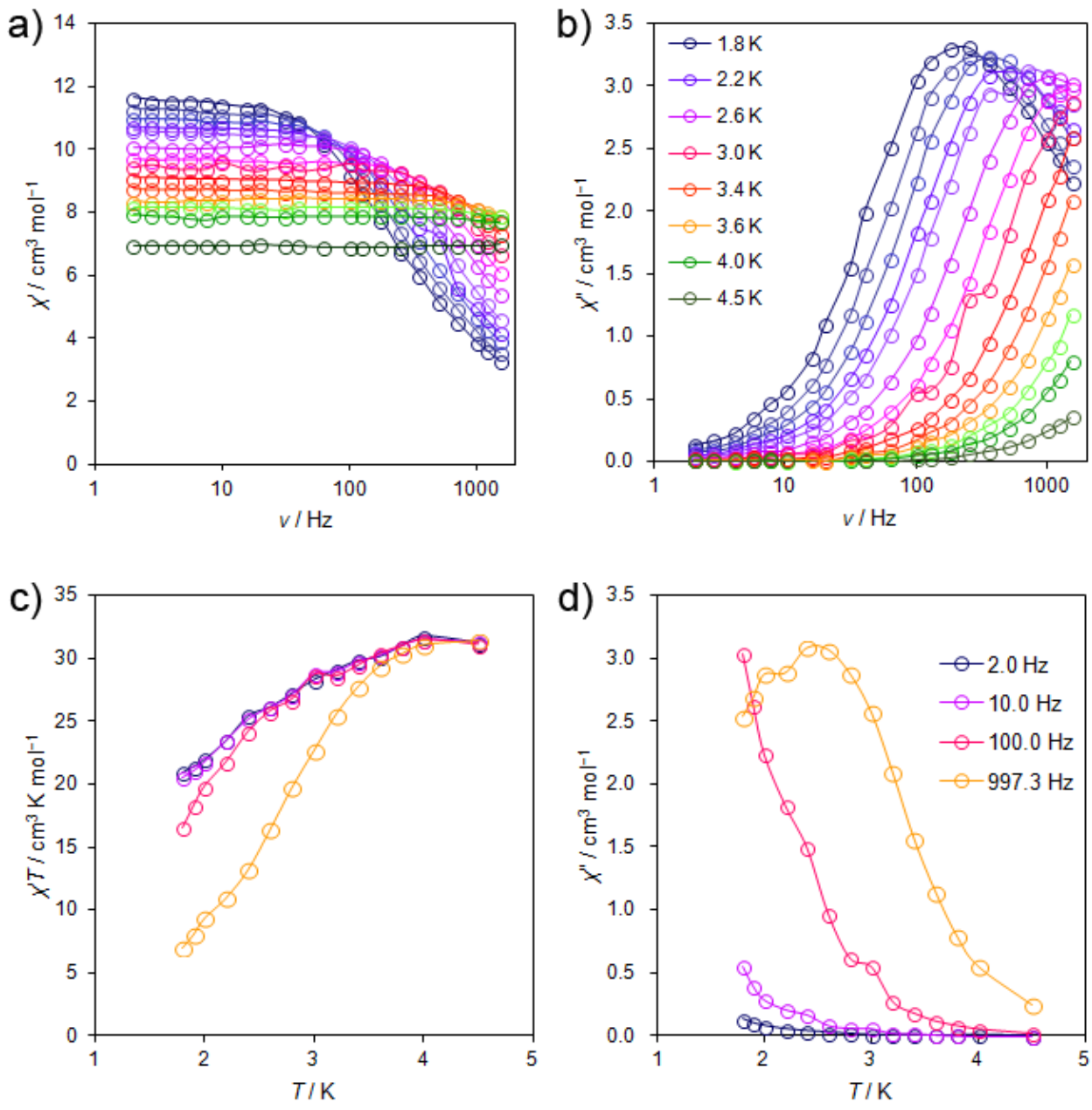

Fig. S16 Frequency dependence of the ac magnetic susceptibility ((a) χ' and (b) χ'') and temperature dependence of the ac magnetic susceptibility ((c) $\chi'T$ and (d) χ'') of $\mathbf{II}_{\mathbf{NiMn4}}$ under the zero external dc field.

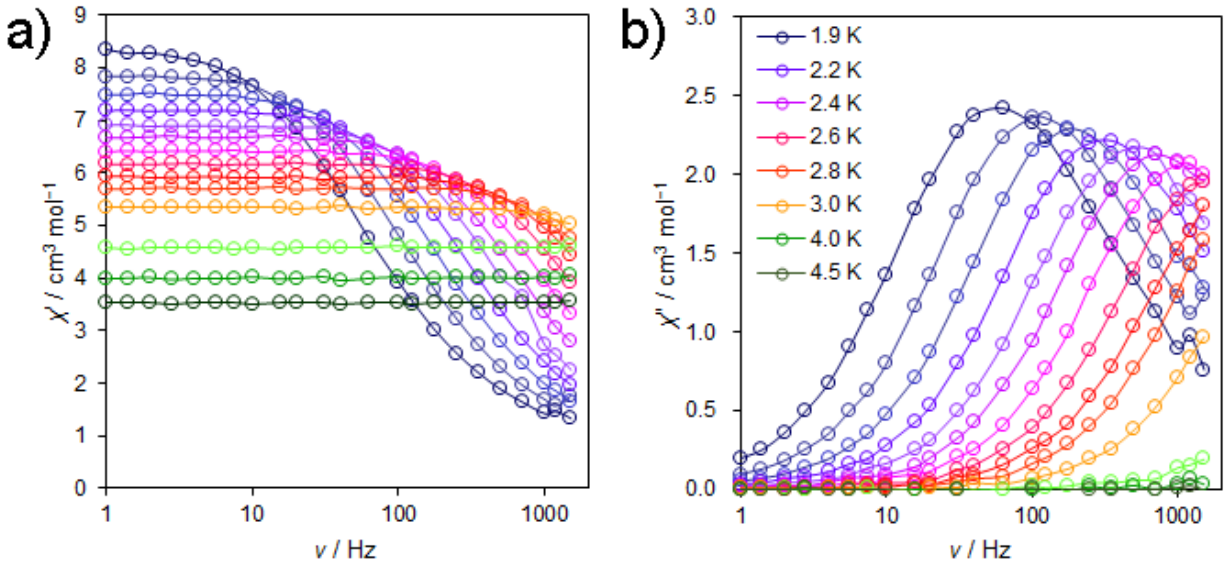

Fig. S17 Frequency dependence of the ac magnetic susceptibility ((a) χ' and (b) χ'') of $\mathbf{II}_{\mathbf{CuMn4}}$ under the zero external dc field.

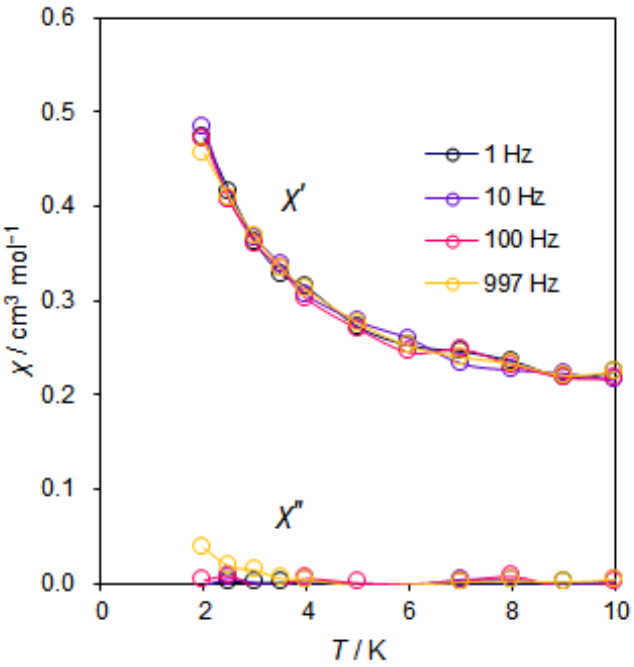

Fig. S18 Temperature dependence of the ac magnetic susceptibility χ' and χ'' of $\mathbf{II}_{\mathbf{GaMn4}}$ under the zero external dc field.

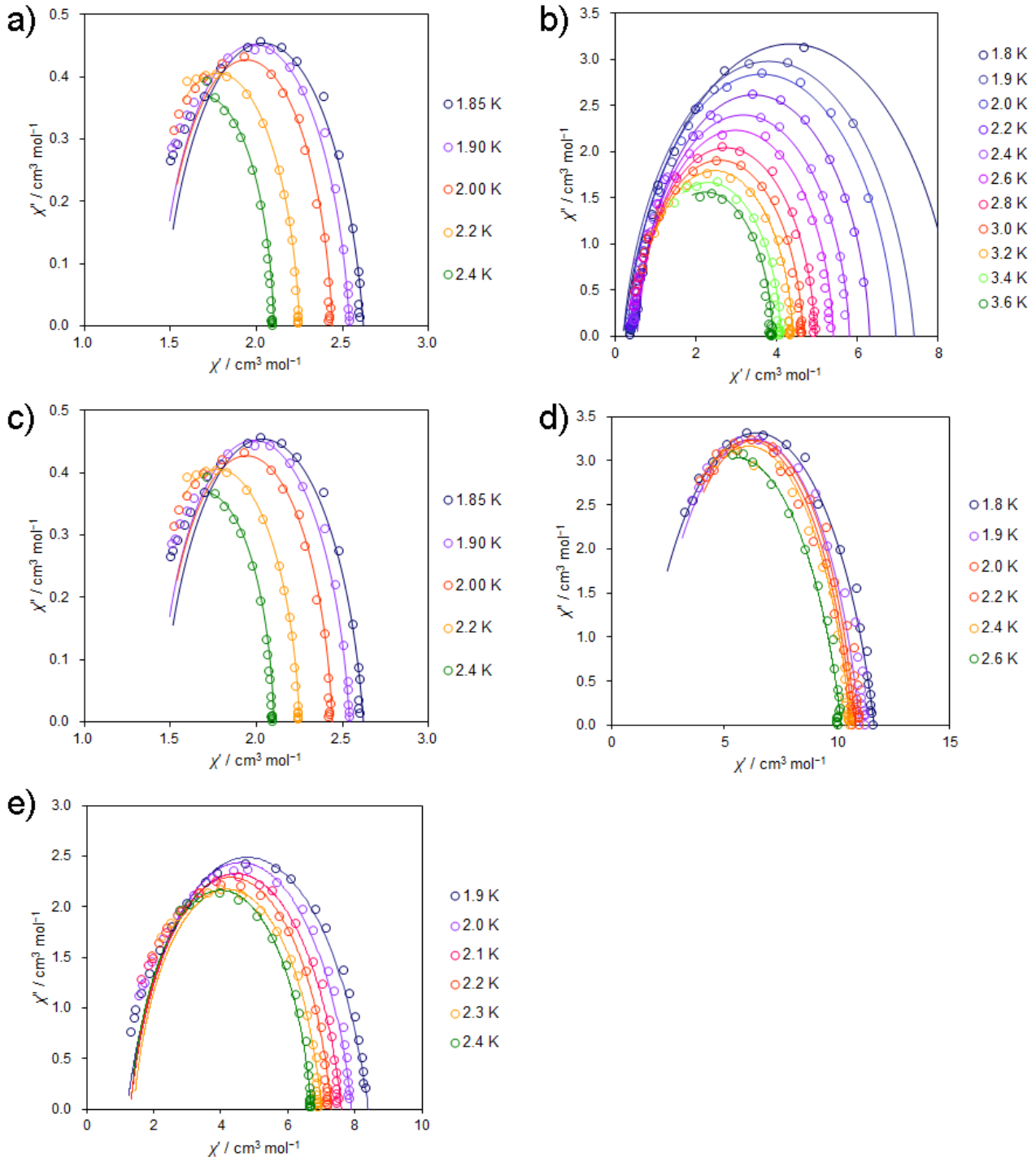

Fig. S19 Cole-Cole plots for ac magnetic susceptibility of (a) **Mn5**, (b) $\mathbf{II}_{\mathbf{FeMn4}}$, (c) $\mathbf{II}_{\mathbf{CoMn4}}$, (d) $\mathbf{II}_{\mathbf{NiMn4}}$, and (e) $\mathbf{II}_{\mathbf{CuMn4}}$. The solid curves are theoretical calculations on the basis of the generalized Debye model.

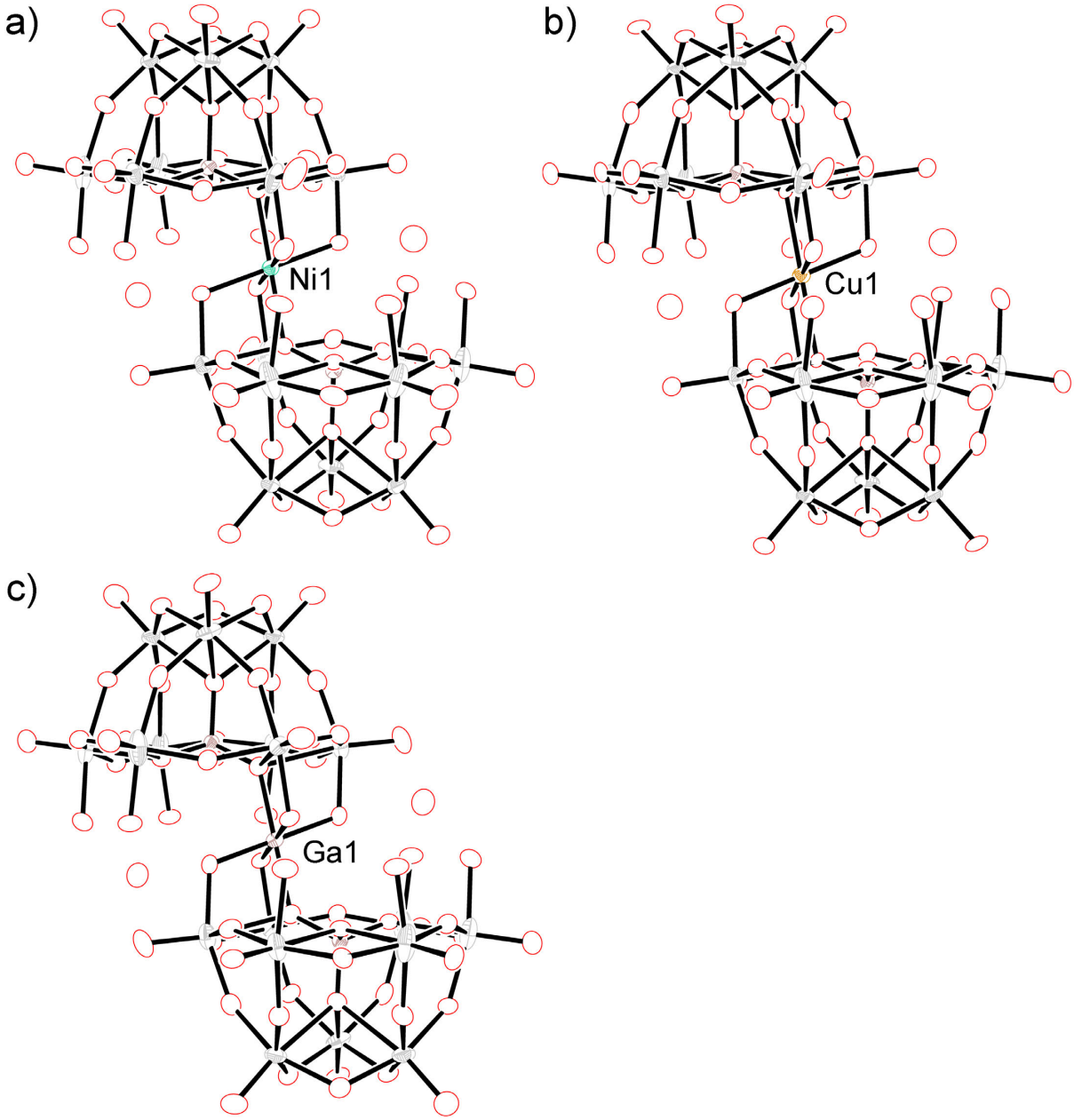

Fig. S20 ORTEP representations of the anion parts of (a) $\mathbf{I_{Ni}}$, (b) $\mathbf{I_{Cu}}$, and (c) $\mathbf{I_{Ga}}$ with thermal ellipsoids drawn at the 50% probably level.

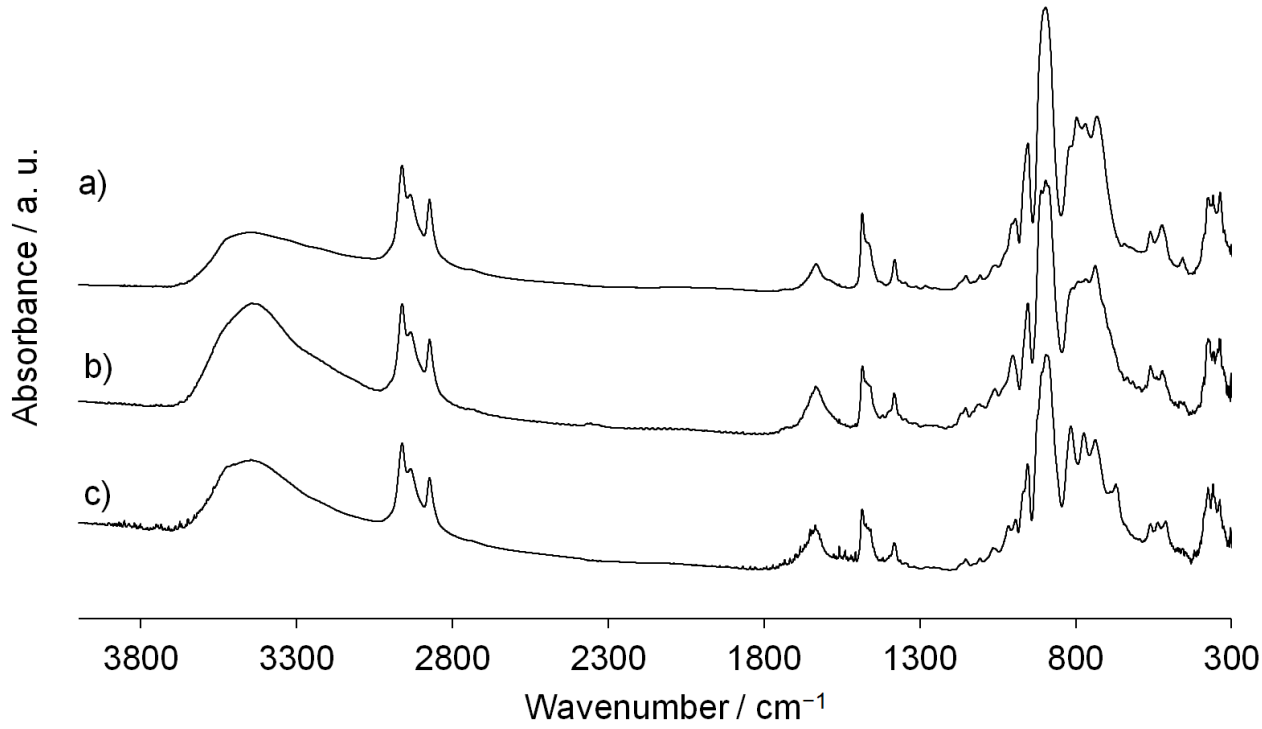

Fig. S21 IR spectra of (a) $\mathbf{I_{Ni}}$, (b) $\mathbf{I_{Cu}}$, and (c) $\mathbf{I_{Ga}}$.

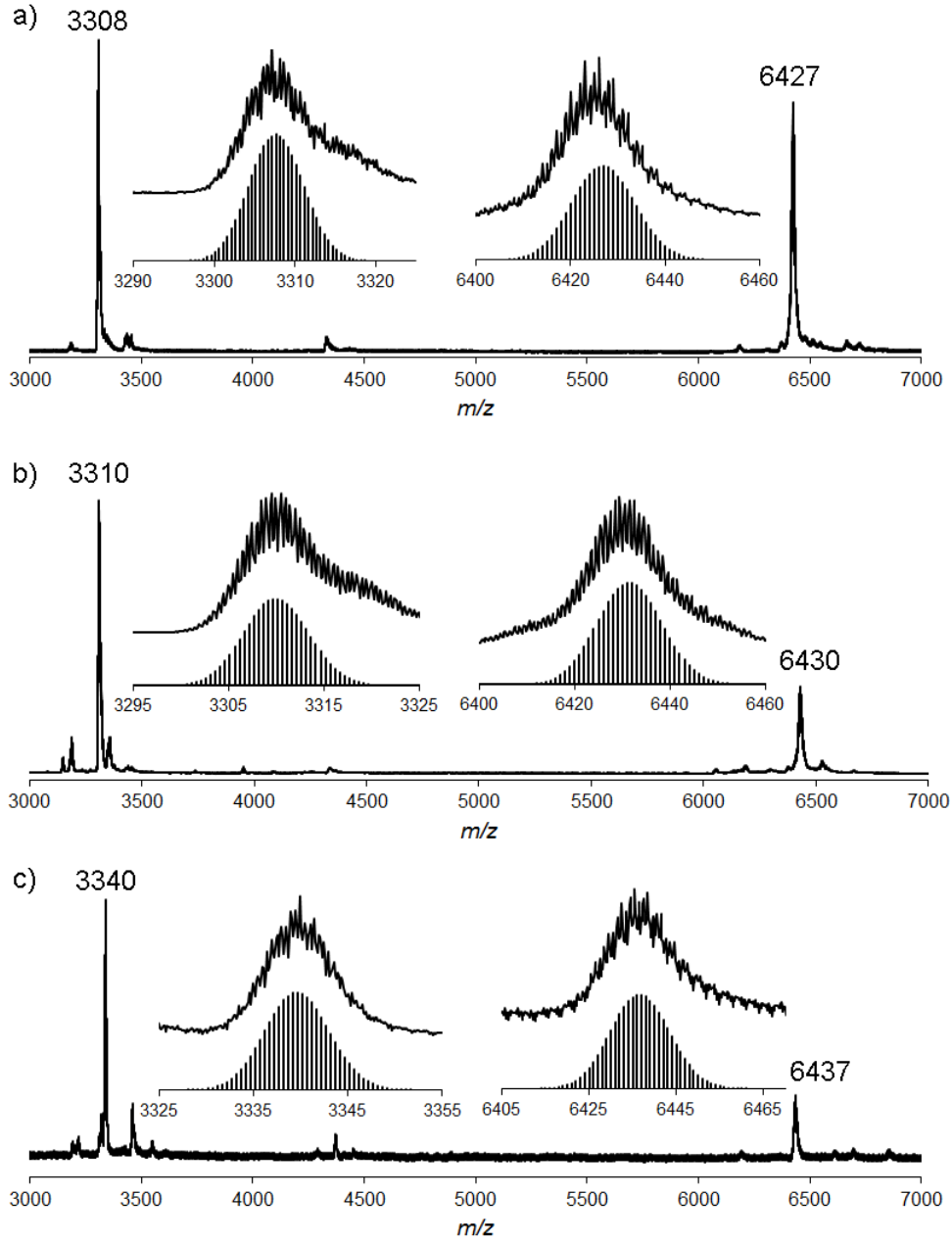

Fig. S22 Positive-ion CSI-mass spectra of (a) $\mathbf{I_{Ni}}$, (b) $\mathbf{I_{Cu}}$, and (b) $\mathbf{I_{Ga}}$ in 1,2-dichloroethane. Inset: (a) spectra in the range of *m/z* 3290–3325 and 6400–6460 and simulated patterns for $[TBA_9HCo(SiW_9O_{31})(SiW_9O_{32})]^{2+}$ (*m/z* 3308) and $[TBA_8H_7Co(SiW_9O_{33})_2]^{+}$ (*m/z* 6427), (b) spectra in the range of *m/z* 3295–3325 and 6400–6460 and simulated patterns for $[TBA_9HCu(SiW_9O_{31})(SiW_9O_{32})]^{2+}$ (*m/z* 3310) and $[TBA_8H_7Cu(SiW_9O_{33})_2]^{+}$ (*m/z* 6430), and (c) spectra in the range of *m/z* 3325–3355 and 6405–6460 and simulated patterns for $[TBA_9H_6Ga(SiW_9O_{33})_2]^{2+}$ (*m/z* 3340) and $[TBA_8H_6Ga(SiW_9O_{33})_2]^{+}$ (*m/z* 6437).

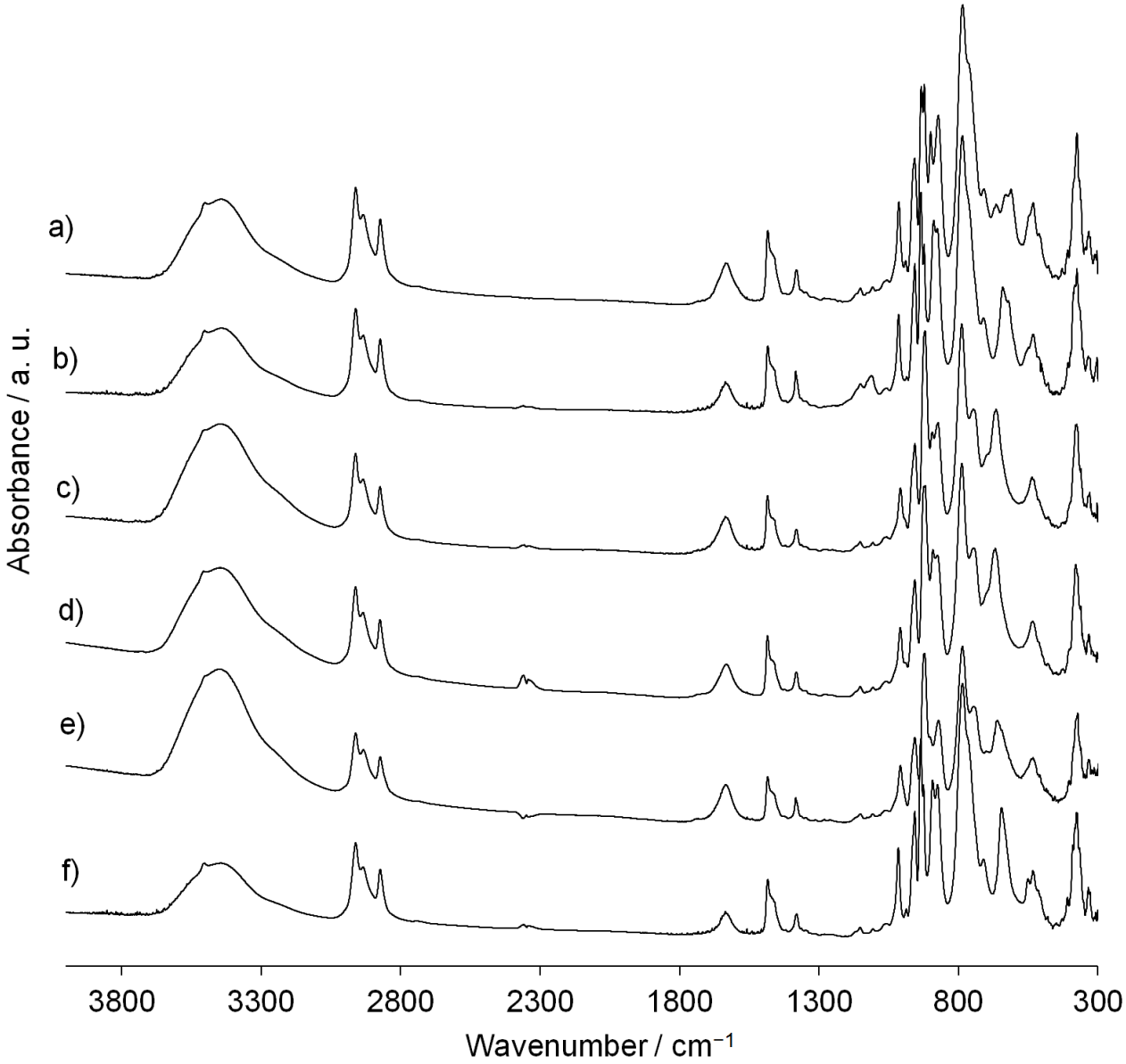

Fig. S23 IR spectra of (a) **Mn5**, (b) $\mathbf{II}_{\mathbf{FeMn4}}$, (c) $\mathbf{II}_{\mathbf{CoMn4}}$, (d) $\mathbf{II}_{\mathbf{NiMn4}}$, (e) $\mathbf{II}_{\mathbf{CuMn4}}$, and (f) $\mathbf{II}_{\mathbf{GaMn4}}$.

Additional references

S1 (*a*) I. D. Brown and D. Altermatt, *Acta Crystallogr.*, 1985, **B41**, 244; (*b*) N. E. Brese and M. O'Keeffe, *Acta Crystallogr.* 1991, **B47**, 192.